Series solutions for spatially coupled buckling anlaysis of thin-walled Timoshenko curved beam on elastic foundation

Nam-Il Kim[†]

*Department of Civil and Environmental Engineering, Myongji University,
San 38-2, Nam-Dong, Yongin, Kyonggi-Do, 449-728, Korea*

Abstract. The spatially coupled buckling, in-plane, and lateral bucking analyses of thin-walled Timoshenko curved beam with non-symmetric, double-, and mono-symmetric cross-sections resting on elastic foundation are performed based on series solutions. The stiffness matrices are derived rigorously using the homogeneous form of the simultaneous ordinary differential equations. The present beam formulation includes the mechanical characteristics such as the non-symmetric cross-section, the thickness-curvature effect, the shear effects due to bending and restrained warping, the second-order terms of semi-tangential rotation, the Wagner effect, and the foundation effects. The equilibrium equations and force-deformation relationships are derived from the energy principle and expressions for displacement parameters are derived based on power series expansions of displacement components. Finally the element stiffness matrix is determined using force-deformation relationships. In order to verify the accuracy and validity of this study, the numerical solutions by the proposed method are presented and compared with the finite element solutions using the classical isoparametric curved beam elements and other researchers' analytical solutions.

Keywords: buckling analysis; curved beam; thin-walled; shear deformation; elastic foundation.

1. Introduction

It is well known that curved beam structures have been used in many civil, mechanical, and aerospace engineering applications such as curved wire, curved girder bridges, turbomachinery blade, tire dynamic, and stiffeners in aircraft structures. It can also be used as a simplified model for a shell structure. The curved beam with thin-walled cross-sections, such as I-section, channel, and angle, are appealing because they offer a high performance in terms of minimum weight for given strength. However, such weight-optimized members having arbitrary cross-section are highly susceptible to buckling and shows very complex behavior due to the coupling effect of axial, flexural and torsional deformation. Therefore, the accurate prediction of their stability limit state is of fundamental importance in the design of thin-walled curved beam structures.

---

† Research Professor, Ph.D., E-mail: kni8501@gmail.com

    Up to the present, a large amount of work was devoted to the improvement of thin-walled curved beam element and the investigation of the stability and vibration behaviors since the early works of Vlasov (1961) and Timoshenko and Gere (1961). Vlasov (1961) formulated the stability equations by substituting the curvature terms of the curved beam into the straight beam equilibrium equation and Timoshenko and Gere (1961) derived the governing equations for buckling of curved beam neglecting the effect of warping. Many researchers (Kim *et al.* 2005, Kim *et al.* 2000a, Wilson and Lee, 1995, Wilson *et al.* 1994, Rajasekaran and Padmanabhan 1989, Papangelis and Trahair 1987, Trahair and Papangelis 1987, Dabrowski 1968, Heins 1975) presented the analytical formulations including closed-form solutions and discussing their results on stability or vibration of curved beams. In the study by Kim *et al.* (2005), the elastic strain energy considering shear effects due to the bending and the non-uniform torsion and the geometric potential energy due to an initial axial force were derived and the closed-form solutions were evaluated for in-plane and out-of-plane buckling loads of thin-walled curved beam. However, in their study, the extensibility of beam axis in evaluation of in-plane buckling loads was neglected.

    On the other hand, the finite element method has been widely used because of its versatility and accordingly considerable research efforts have been made to obtain acceptable results for the coupled behavior of curved structures. Choi and Hong (2001) performed the static analysis of single- and multi-span curved box girder bridges using the modified finite strip method. Chucheepsakul and Saetiew (2002) presented a finite element approach for determining the natural frequencies for planar arches of various shapes vibrating in three- dimensional space. In their study, displacement components were expressed by cubic polynomials in terms of the arc length parameter. Chang *et al.* (1996) presented numerical solutions on spatial stability of the circular arch using the thin-walled straight beam element based on cubic Hermitian polynomials. Usuki *et al.* (1979) and Watanabe *et al.* (1982) developed the lateral-torsional buckling theory together with the finite element formulation of thin-walled circular arch accounting for prebuckling deflections. In spatial stability analysis of curved beam, the non-commutative nature of rotations about different axes and deficiency of the equilibrium condition along the finite curved length when considering internal moments as quasi-tangential moments render the analysis more complicated. In order to resolve these problems, Kim *et al.* (2003), Kim *et al.* (2000b), Hu *et al.* (1999), and Saleeb and Gendy (1991) introduced the improved displacement field adding the second-order terms of finite rotations to the displacement field of curved beam and performed the stability analysis using the finite element method.

    The complicated problems for the analysis of curved beam on elastic foundation are frequently encountered due to additional parameters related to the foundation effects. There exists a wide body of literature on the analysis of beams resting on elastic foundation since the early works of Hetenyi (1946) who developed the differential equation approach. Lee *et al.* (2002) derived the governing differential equations for the out-of-plane free vibration of circular curved beams resting on Winkler-type foundations and solved numerically using the Runge-Kutta method. Wang and Brannen (1982) studied the effects of Winkler-Pasternak foundations upon natural frequencies of circular curved beams out of their initial plane of curvature. Rodriquez (1961) derived the closed-form solutions of differential equations of circular beam on elastic foundation. Also the finite element formulations which are based on displacement types have been developed by Sengupta and Dasgupta (1987) and Banan *et al.* (1989). Aköz and Kadioğlu (1996) developed the mixed finite element formulation for circular beams on Winkler foundation. Chakraborty and Sarkar (2000) presented a stochastic finite element method for analysis of a curved beam on uncertain elastic

foundation. In their study, the finite element solution was obtained utilizing the Neumann expansion method within the framework of Monte Carlo simulation.

From the previously cited references, it can be noted that even though a significant amount of research has been extensively conducted on development of a stability analysis of curved beam, to the best of authors' knowledge, there still has been no study reported in the literature on the evaluation of the spatially coupled buckling loads of thin-walled Timoshenko curved beam with non-symmetric cross-section resting on elastic foundation. It is well known that the stability behavior of thin-walled curved beam with non-symmetric cross- section is very complex due to the coupling effect of axial, flexural and torsional deformation and many researchers thought that it is difficult to solve the spatially coupled stability problem of curved beam analytically.

The aim of this study is to present, the stiffness matrices for the spatially coupled buckling, in-plane, and lateral bucking analyses of thin-walled Timoshenko curved beam with non-symmetric, double-, and mono-symmetric cross-sections resting on two-types of elastic foundation using the power series method. The important points of the present study are summarized as follows:

1. The equilibrium equations and the force-deformation relations of the curved beam on two-types of elastic foundation considering the shear effects are derived from the total potential energy.
2. Based on the power series expansions of displacement components, the stiffness matrix for coupled stability analysis of beam with non-symmetric cross-section on elastic foundation is evaluated.
3. As special cases, the stiffness matrices for in-plane bucking analysis of curved beam allowing the extension along the beam axis in potential energy and for lateral buckling analysis of beam with double- and mono-symmetric cross-sections are evaluated.
4. To demonstrate the accuracy and the validity of this study, the numerical solutions by the present approach are presented and compared with the finite element solutions using the classical isoparametric curved beam elements and other researchers' solutions.
5. The coupling and crossover phenomena of symmetric and anti-symmetric buckling modes with changes in curvature and subtended angle are investigated.

2. Stability theory of thin-walled Timoshenko curved beam

Fig. 1 shows the global curvilinear coordinate system (x_1, x_2, x_3) of the curved beam in which the x_1 axis coincides with a centroid axis having the radius of curvature R but x_2, x_3 are not necessarily principal inertia axes. The displacement parameters and the stress resultants of the thin-walled curved beams defined at the non-symmetric cross-section are presented in Figs. 2(a) and 2(b), respectively, in which U_x, U_y, U_z, and ω_1, ω_2, ω_3 are the rigid body translations and the rotations of beam with respect to x_1, x_2, and x_3 axes, respectively; f is the displacement parameter measuring warping deformations. Also F_1, F_2, and F_3 are the axial and shear forces, respectively, acting at the centroid; M_1 is the total twisting moment with respect to the centroid axis; M_2 and M_3 are the bending moments with respect to x_2 and x_3 axes, respectively; M_ϕ is the bimoment; x_2^p and x_3^p mean principal axes defined at the centroid in which θ is the angle between x_2^p and x_2 axes in the counterclockwise direction. Assuming that the cross-section is rigid in its own plane, the total displacement field can be written as follows:
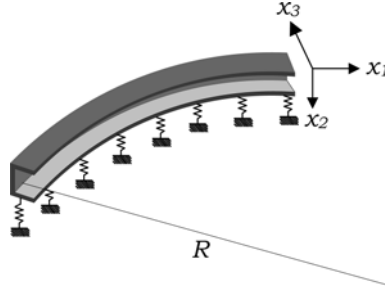
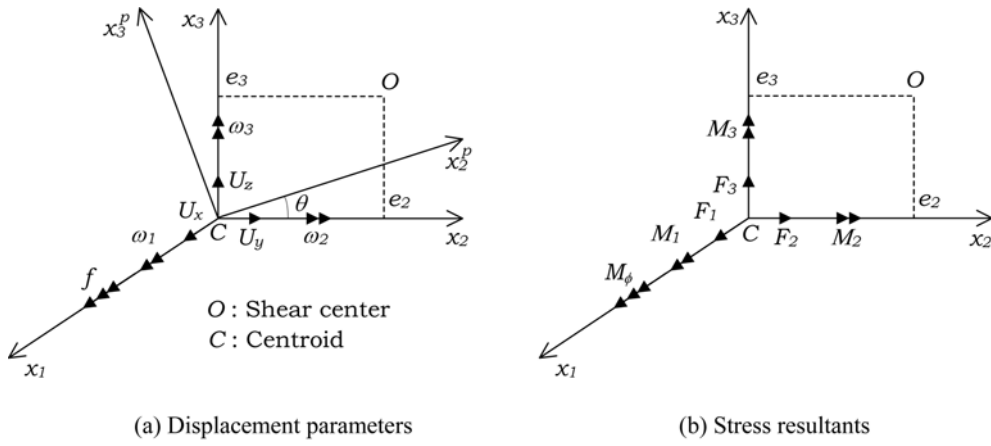Fig. 1 Curvilinear coordinate system of a thin-walled curved beam

(a) Displacement parameters   (b) Stress resultants

Fig. 2 Notation for displacement parameters and stress resultants

$$U_1 = U_x - x_2\omega_3 + x_3\omega_2 + f\phi \tag{1a}$$

$$U_2 = U_y - x_3\omega_1 \tag{1b}$$

$$U_3 = U_z + x_2\omega_1 \tag{1c}$$

where ϕ is the normalized warping function defined at the centroid and the following relationship between ϕ and ϕ^s defined at the shear center is obtained.

$$\phi = \phi^s + e_2 x_3 - e_3 x_2 \tag{2}$$

In Eq. (2), (e_2, e_3) denotes the position vector of the shear center. The stress resultants with respect to the centroid are as follows

$$F_1 = \int_A \tau_{11} dA, \; F_2 = \int_A \tau_{12} dA, \; F_3 = \int_A \tau_{13} dA, \; M_1 = \int_A (\tau_{13} x_2 - \tau_{12} x_3) dA$$

$$M_2 = \int_A \tau_{11} x_3 dA, \; M_3 = -\int_A \tau_{11} x_2 dA, \; M_\phi = \int_A \tau_{11} \phi \, dA, \; M_P = \int_A \tau_{11} (x_2^2 + x_3^2) dA$$

$$M_R = \int_A \left[\tau_{12} \phi_{,2} + \tau_{13} \left(\phi_{,3} - \frac{\phi}{R + x_3} \right) \right] \frac{R + x_3}{R} dA \tag{3a-i}$$

In Eqs. (3h, i), M_P and M_R are the stress resultant known as the Wagner effect and the restrained torsional moment, respectively; The ', 2' and ', 3' denote differentiation with respect to the x_2 and x_3, respectively. The St. Venant torsional moment is expressed as

$$M_{st} = M_1 - M_R = M_1 - M'_\phi = GJ\left(\omega'_1 + \frac{\omega_3}{R}\right) \tag{4}$$

where G and J are the shear modulus and the torsional constant, respectively and the prime denotes differentiation with respect to the position x_1. For later use, the sectional properties are defined by

$$I_2 = \int_A x_3^2 dA, \; I_3 = \int_A x_2^2 dA, \; I_{23} = \int_A x_2 x_3 dA, \; I_\phi = \int_A \phi^2 dA, \; I_{\phi 2} = \int_A \phi x_3 dA$$

$$I_{\phi 3} = \int_A \phi x_2 dA, \; I_{222} = \int_A x_3^3 dA, \; I_{223} = \int_A x_2 x_3^2 dA, \; I_{233} = \int_A x_2^2 x_3 dA$$

$$I_{333} = \int_A x_2^3 dA, \; I_{\phi 22} = \int_A \phi x_3^2 dA, \; I_{\phi 23} = \int_A \phi x_2 x_3 dA, \; I_{\phi 33} = \int_A \phi x_2^2 dA$$

$$I_{\phi\phi 2} = \int_A \phi^2 x_3 dA, \; I_{\phi\phi 3} = \int_A \phi^2 x_2 dA \tag{5a-o}$$

where I_2, I_3, I_{23}, and I_ϕ are the second moment of inertia about x_2 and x_3 axes, the product moment of inertia, and the warping moment of inertia, respectively; $I_{\phi 2}(=I_2 e_2)$ and $I_{\phi 3}(=-I_3 e_3)$ are the product moments of inertia due to the normalized warping; $I_{ijk}(i,j,k = \phi, 2, 3)$ are the third moments of inertia.

From the study of Kim *et al.* (2005), the elastic strain energy of the thin-walled curved beam considering the non-symmetric cross-section, the shear effects due to bending and non-uniform warping, and the thickness- curvature effect which makes larger difference in the prediction of buckling loads in the curved beam with large subtended angle and small radius, is given as

$$\Pi_E = \frac{1}{2}\int_\ell^l \left[EA\left(U'_x + \frac{U_z}{R}\right)^2 + E\hat{I}_2\left(\omega'_2 - \frac{U'_x}{R} - \frac{U_z}{R^2}\right)^2 + E\hat{I}_3\left(\omega'_3 - \frac{\omega_1}{R}\right)^2 + E\hat{I}_\phi f'^2 \right.$$

$$+ 2E\hat{I}_{\phi 2}\left(\omega'_2 - \frac{U'_x}{R} - \frac{U_z}{R^2}\right)f' - 2E\hat{I}_{\phi 3}\left(\omega'_3 - \frac{\omega_1}{R}\right)f' - 2E\hat{I}_{23}\left(\omega'_3 - \frac{\omega_1}{R}\right)\left(\omega'_2 - \frac{U'_x}{R} - \frac{U_z}{R^2}\right)$$

$$+ GJ\left(\omega'_1 + \frac{\omega_3}{R}\right)^2 + GA_2(U'_y - \omega_3)^2 + GA_3\left(U'_z - \frac{U_x}{R} + \omega_2\right)^2 + GA_r\left(\omega'_1 + \frac{\omega_3}{R} + f\right)^2$$

$$+ 2GA_{23}(U'_y - \omega_3)\left(U'_z - \frac{U_x}{R} + \omega_2\right) + 2GA_{2r}(U'_y - \omega_3)\left(\omega'_1 + \frac{\omega_3}{R} + f\right)$$

$$\left. + 2GA_{3r}\left(U'_z - \frac{U_x}{R} + \omega_2\right)\left(\omega'_1 + \frac{\omega_3}{R} + f\right) \right]dx_1 \tag{6}$$

where

$$\hat{I}_2 = I_2 - \frac{I_{222}}{R}, \quad \hat{I}_3 = I_3 - \frac{I_{233}}{R}, \quad \hat{I}_{23} = I_{23} - \frac{I_{223}}{R}$$

$$\hat{I}_\phi = I_\phi - \frac{I_{\phi\phi 2}}{R}, \quad \hat{I}_{\phi 2} = I_{\phi 2} - \frac{I_{\phi 22}}{R}, \quad \hat{I}_{\phi 3} = I_{\phi 3} - \frac{I_{\phi 23}}{R} \tag{7a-f}$$

In Eq. (5), E and A are the Young's modulus and the cross-sectional area, respectively. The effective shear areas defined between the centroid and the shear center are as follows:

$$A_2 = A_2^s \cos^2\theta + A_3^s \sin^2\theta, \qquad A_3 = A_3^s \cos^2\theta + A_2^s \sin^2\theta$$

$$A_r = A_r^s + A_2^s e_3^2 + A_3^s e_2^2, \qquad A_{23} = (A_2^s + A_3^s)\cos\theta\sin\theta \qquad \text{(8a-f)}$$

$$A_{2r} = -A_2^s e_3 \cos\theta - A_3^s e_2 \sin\theta, \qquad A_{3r} = -A_2^s e_3 \sin\theta + A_3^s e_2 \cos\theta$$

where

$$\frac{1}{A_2^s} = \frac{1}{I_{3p}^2}\int_A Q_3^2 \frac{ds}{t}, \quad \frac{1}{A_3^s} = \frac{1}{I_{2p}^2}\int_A Q_2^2 \frac{ds}{t}, \quad \frac{1}{A_r^s} = \frac{1}{(I_\phi^2)^2}\int_A Q_r^2 \frac{ds}{t} \qquad \text{(9a-c)}$$

And

$$I_{2p} = \int_A (x_3^p)^2 dA, \quad I_{3p} = \int_A (x_2^p)^2 dA, \quad I_\phi^s = \int_A (\phi^s)^2 dA$$

$$Q_2 = \int_o^s x_3^p t\, ds, \quad Q_3 = \int_o^s x_2^p t\, ds, \quad Q_r = \int_o^s \phi^s t\, ds \qquad \text{(10a-f)}$$

where Q_2 and Q_3 are the statical moments of area about x_2 and x_3 axes, respectively; Q_r is the statical warping moment; t and s are the wall thickness and the coordinate along the contour of the cross-section, respectively.

In this study, we consider the thin-walled cross-section resting on elastic foundation, as shown in Fig. 3, throughout its length, in which a more realistic and generalized representation of the elastic foundation can be accomplished by the way of a two-types of foundation model. In Fig. 3, k_y and k_z are the Winkler foundation moduli indicating the first type of foundation parameters for the transverse translations at the point (h_y, h_z); k_ω is the rotational parameter for rotation of the cross-section; g_y and g_z denote the second type of foundation parameters (i.e., Vlasov, Pasternak and Filonenko-Borodich foundation modulus) at the point (h_y, h_z). The strain energy considering the foundation effects are deduced from the study by Dube and Dumir (1996) as follow

$$\Pi_F = \frac{1}{2}\int_o^l [k_y(U_y - h_z\omega_1)^2 + k_z(U_z + h_y\omega_1)^2 + k_\omega\omega_1^2 + g_y(U_y' - h_z\omega_1')^2 + g_z(U_z' + h_y\omega_1')^2] \qquad \text{(11)}$$
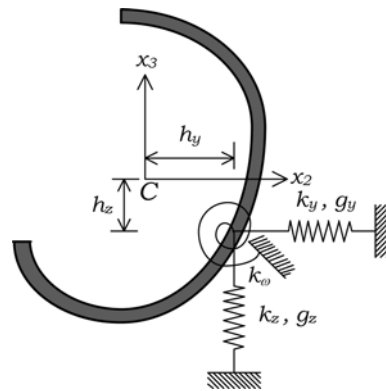

Fig. 3 Cross-section of beam on two-types of elastic foundation

For the stability analysis of curved beam, the potential energy due to the initial axial force $^oF_1$ and bending moment $^oM_2$ including the second-order terms of semi-tangential rotation and the Wagner effect is extracted from the study by Kim *et al.* (2005) as follows

$$\Pi_G = \frac{1}{2}\int_o^l \left[{}^oF_1\left\{\left(U_x' + \frac{U_z}{R}\right)^2 + U_y'^2 + \left(U_z' - \frac{U_x}{R}\right)^2\right\} + {}^oM_2\left\{2\omega_2'\left(U_x' + \frac{U_z}{R}\right) - \frac{1}{R}\left(U_x' + \frac{U_z}{R}\right)^2\right.\right.$$
$$\left.\left. + \omega_1'\omega_3 + \omega_1\omega_3' - \frac{1}{R}(U_y'^2 + \omega_1^2) - 2U_y'\omega_1' - \frac{1}{R}\left(\omega_2 + U_z' - \frac{U_x}{R}\right)^2\right\} + (\beta_1{}^oF_1 + \beta_2{}^oM_2)\left(\omega_1' + \frac{\omega_3}{R}\right)^2\right]dx_1 \tag{12}$$

where the coefficients β_1 and β_2 can be obtained from

$$\begin{bmatrix} A + \dfrac{\hat{I}_2}{R^2} & -\dfrac{\hat{I}_2}{R} \\ -\dfrac{\hat{I}_2}{R} & \hat{I}_2 \end{bmatrix} \begin{Bmatrix} \beta_1 \\ \beta_2 \end{Bmatrix} = \begin{Bmatrix} \hat{I}_2 + \hat{I}_3 \\ I_{222} + I_{233} \end{Bmatrix} \tag{13}$$

Consequently, the total potential energy functional of a thin-walled Timoshenko curved beam resting on elastic foundation is expressed as follows

$$\Pi = \Pi_E + \Pi_G + \Pi_F - \Pi_{ext} \tag{14}$$

where Π_{ext} is the potential energy due to the element nodal forces.

By taking the variation of Eq. (14) with respect to seven displacement parameters, U_x, U_y, U_z, ω_1, ω_2, ω_3, and f, the coupled equilibrium equations and force-deformation relations for the curved beam are derived as follows

$$-EA\left(U_x'' + \frac{U_z'}{R}\right) + \frac{1}{R}E\hat{I}_2\left(\omega_2'' - \frac{U_x''}{R} - \frac{U_z'}{R^2}\right) + \frac{1}{R}E\hat{I}_{\phi 2}f'' - \frac{1}{R}E\hat{I}_{23}\left(\omega_3'' - \frac{\omega_1'}{R}\right)$$
$$-\frac{1}{R}GA_3\left(U_z' + \omega_2 - \frac{U_x}{R}\right) - \frac{1}{R}GA_{23}\left(U_y' - \omega_3\right) - \frac{1}{R}GA_{3r}\left(\omega_1' + f + \frac{\omega_3}{R}\right) \tag{15a}$$
$$-{}^oF_1\left\{\left(U_x'' + \frac{U_z'}{R}\right) + \frac{1}{R}\left(U_z' - \frac{U_x}{R}\right)\right\} - {}^oM_2\left\{\omega_2'' - \frac{1}{R}\left(U_x'' + \frac{U_z'}{R}\right) - \frac{1}{R^2}\left(\omega_2 + U_z' - \frac{U_x}{R}\right)\right\} = 0$$

$$GA_2\left(U_y'' - \omega_3'\right) + GA_{23}\left(U_z'' + \omega_2' - \frac{U_x'}{R}\right) + GA_{2r}\left(\omega_1'' + f' + \frac{\omega_3'}{R}\right)$$
$$-k_y\left(U_y - h_z\omega_1\right) + g_y\left(U_y'' - h_z\omega_1''\right) + {}^oF_1U_y'' - {}^oM_2\left(\omega_1'' + \frac{U_y''}{R}\right) = 0 \tag{15b}$$

$$\frac{1}{R}EA\left(U_x' + \frac{U_z}{R}\right) - \frac{1}{R^2}E\hat{I}_2\left(\omega_2' - \frac{U_x'}{R} - \frac{U_z}{R^2}\right) - \frac{1}{R^2}E\hat{I}_{\phi 2}f' + \frac{1}{R^2}E\hat{I}_{23}\left(\omega_3' - \frac{\omega_1}{R}\right)$$
$$-GA_3\left(U_z'' + \omega_2' - \frac{U_x'}{R}\right) - GA_{23}\left(U_y'' - \omega_3'\right) - GA_{3r}\left(\omega_1'' + f' + \frac{\omega_3'}{R}\right) + k_z\left(U_z + h_y\omega_1\right) - g_z\left(U_z'' + h_y\omega_1''\right) \tag{15c}$$
$$+{}^oF_1\left\{\frac{1}{R}\left(U_x' + \frac{U_z}{R}\right) - \left(U_z'' - \frac{U_x'}{R}\right)\right\} + {}^oM_2\left\{\frac{\omega_2'}{R} - \frac{1}{R^2}\left(U_x' + \frac{U_z}{R}\right) + \frac{1}{R}\left(\omega_2' + U_z'' - \frac{U_x'}{R}\right)\right\} = 0$$

$$-\frac{1}{R}E\hat{I}_3\left(\omega_3'-\frac{\omega_1}{R}\right)+\frac{1}{R}E\hat{I}_{\phi3}f'+\frac{1}{R}E\hat{I}_{23}\left(\omega_2'-\frac{U_x'}{R}-\frac{U_z}{R^2}\right)-GJ\left(\omega_1''+\frac{\omega_3'}{R}\right)-GA_r\left(\omega_1''+f'+\frac{\omega_3'}{R}\right)$$

$$-GA_{2r}\left(U_y''-\omega_3'\right)-GA_{3r}\left(U_z''+\omega_2'-\frac{U_x'}{R}\right)-k_yh_zU_y+k_zh_yU_z+\left(k_yh_z^2+k_zh_y^2+k_\omega\right)\omega_1 \tag{15d}$$

$$+g_yh_zU_y''-g_zh_yU_z''-\left(g_yh_z^2+g_zh_y^2\right)\omega_1''-\beta_1{}^oF_1\left(\omega_1''+\frac{\omega_3'}{R}\right)+{}^oM_2\left\{U_y''-\frac{\omega_1}{R}-\beta_2\left(\omega_1''+\frac{\omega_3'}{R}\right)\right\}\Biggr\}=0$$

$$-E\hat{I}_2\left(\omega_2''-\frac{1}{R}U_x''-\frac{1}{R^2}U_z'\right)-E\hat{I}_{\phi2}f''+E\hat{I}_{23}\left(\omega_3''-\frac{1}{R}\omega_1'\right)+GA_3\left(U_z'+\omega_2-\frac{1}{R}U_x\right)$$

$$+GA_{23}\left(U_y'-\omega_3\right)+GA_{3r}\left(\omega_1'+f+\frac{1}{R}\omega_3\right)-{}^oM_2\left\{\left(U_x''+\frac{U_z'}{R}\right)+\frac{1}{R}\left(\omega_2+U_z'-\frac{U_x}{R}\right)\right\}=0 \tag{15e}$$

$$-E\hat{I}_3\left(\omega_3''-\frac{1}{R}\omega_1'\right)+E\hat{I}_{\phi3}f''+E\hat{I}_{23}\left(\omega_2''-\frac{1}{R}U_x''-\frac{1}{R^2}U_z'\right)+\frac{1}{R}GJ\left(\omega_1'+\frac{1}{R}\omega_3\right)-GA_2\left(U_y'-\omega_3\right)$$

$$-GA_{23}\left(U_z'+\omega_2-\frac{1}{R}U_x\right)+\frac{1}{R}GA_r\left(\omega_1'+f+\frac{1}{R}\omega_3\right)-GA_{2r}\left(\omega_1'+f-\frac{1}{R}U_y'+\frac{2}{R}\omega_3\right) \tag{15f}$$

$$+\frac{1}{R}GA_{3r}\left(U_z'+\omega_2-\frac{1}{R}U_x\right)+{}^oF_1\frac{\beta_1}{R}\left(\omega_1'+\frac{\omega_3}{R}\right)+{}^oM_2\frac{\beta_2}{R}\left(\omega_1'+\frac{\omega_3}{R}\right)=0$$

$$-E\hat{I}_\phi f''-E\hat{I}_{\phi2}\left(\omega_2''-\frac{1}{R}U_x''-\frac{1}{R^2}U_z'\right)+E\hat{I}_{\phi3}\left(\omega_3''-\frac{1}{R}\omega_1'\right)+GA_r\left(\omega_1'+f+\frac{1}{R}\omega_3\right)$$

$$+GA_{2r}\left(U_y'-\omega_3\right)+GA_{3r}\left(U_z'+\omega_2-\frac{1}{R}U_x\right)=0 \tag{15g}$$

And force-deformation relations are

$$F_1=EA\left(U_x'+\frac{U_z}{R}\right)-\frac{1}{R}E\hat{I}_2\left(\omega_2'-\frac{U_x'}{R}-\frac{U_z}{R^2}\right)-\frac{1}{R}E\hat{I}_{\phi2}f'+\frac{1}{R}E\hat{I}_{23}\left(\omega_3'-\frac{\omega_1}{R}\right)$$

$$+{}^oF_1\left(U_x'+\frac{U_z}{R}\right)+{}^oM_2\left\{\omega_2'-\frac{1}{R}\left(U_x'+\frac{U_z}{R}\right)\right\} \tag{16a}$$

$$F_2=GA_2\left(U_y'-\omega_3\right)+GA_{23}\left(U_z'+\omega_2-\frac{U_x}{R}\right)+GA_{2r}\left(\omega_1'+f+\frac{\omega_3}{R}\right)+g_y\left(U_y'-h_z\omega_1'\right)$$

$$+{}^oF_1U_y'-{}^oM_2\left(\omega_1'+\frac{U_y'}{R}\right) \tag{16b}$$

$$F_3=GA_3\left(U_z'+\omega_2-\frac{U_x}{R}\right)+GA_{23}\left(U_y'-\omega_3\right)+GA_{3r}\left(\omega_1'+f+\frac{\omega_3}{R}\right)+g_z\left(U_z'+h_y\omega_1'\right)$$

$$+{}^oF_1\left(U_z'-\frac{U_x}{R}\right)-\frac{1}{R}{}^oM_2\left(\omega_2+U_z'-\frac{U_x}{R}\right) \tag{16c}$$

$$M_1 = GJ\left(\omega_1' + \frac{\omega_3}{R}\right) + GA_r\left(\omega_1' + f + \frac{\omega_3}{R}\right) + GA_{2r}\left(U_y' - \omega_3\right) + GA_{3r}\left(U_z' + \omega_2 - \frac{U_x}{R}\right) - g_y h_z U_y'$$

$$+ g_z h_y U_z' - \left(g_y h_z^2 + g_z h_y^2\right)\omega_1' + \beta_1\,^oF_1\left(\omega_1' + \frac{\omega_3}{R}\right) + \,^oM_2\left\{0.5\omega_3 - U_y' + \beta_2\left(\omega_1' + \frac{\omega_3}{R}\right)\right\} \tag{16d}$$

$$M_2 = E\hat{I}_2\left(\omega_2' - \frac{U_x'}{R} - \frac{U_z}{R^2}\right) + E\hat{I}_{\phi 2}f' - E\hat{I}_{23}\left(\omega_3' - \frac{\omega_1}{R}\right) + \,^oM_2\left(U_x' + \frac{U_z}{R}\right) \tag{16e}$$

$$M_3 = E\hat{I}_3\left(\omega_3' - \frac{\omega_1}{R}\right) - E\hat{I}_{\phi 3}f' - E\hat{I}_{23}\left(\omega_2' - \frac{U_x'}{R} - \frac{U_z}{R^2}\right) + 0.5\,^oM_2\omega_1 \tag{16f}$$

$$M_\phi = E\hat{I}_\phi f' + E\hat{I}_{\phi 2}\left(\omega_2' - \frac{U_x'}{R} - \frac{U_z}{R^2}\right) - E\hat{I}_{\phi 3}\left(\omega_3' - \frac{\omega_1}{R}\right) \tag{16g}$$

3. Element stiffness matrices of curved beam

3.1 Stiffness matrix for spatially coupled buckling of curved beam

In this subsection, for the spatially coupled stability analysis of thin-walled Timoshenko curved beam resting on elastic foundation, the element stiffness matrix is evaluated rigorously from the equilibrium equations and the force-deformation relations derived in previous section.

3.1.1 Evaluation of displacement functions

For the evaluation of displacement functions of the curved beam, the following displacement state vector consisting of 14 displacement parameters is considered.

$$\mathbf{d} = <U_x, U_x', U_y, U_y', U_z, U_z', \omega_1, \omega_1', \omega_2, \omega_2', \omega_3, \omega_3', f, f'>^T \tag{17}$$

The solutions of seven displacement parameters are taken as the following infinite power series.

$$U_x = \sum_{n=0}^{\infty} a_n x^n, \qquad U_y = \sum_{n=0}^{\infty} b_n x^n, \qquad U_z = \sum_{n=0}^{\infty} c_n x^n$$

$$\omega_1 = \sum_{n=0}^{\infty} d_n x^n, \quad \omega_2 = \sum_{n=0}^{\infty} e_n x^n, \quad \omega_3 = \sum_{n=0}^{\infty} f_n x^n, \quad f = \sum_{n=0}^{\infty} g_n x^n \tag{18a-g}$$

Substituting Eqs. (18a-g) into Eqs. (15a-g), the equilibrium equations can be expressed as

$$-EA\left\{\sum_{n=2}^{\infty} n(n-1)a_n x^{n-2} + \frac{1}{R}\sum_{n=1}^{\infty} nc_n x^{n-1}\right\} + \frac{E\hat{I}_2}{R}\left\{\sum_{n=2}^{\infty} n(n-1)e_n x^{n-2} - \frac{1}{R}\sum_{n=2}^{\infty} n(n-1)a_n x^{n-2} - \frac{1}{R^2}\sum_{n=1}^{\infty} nc_n x^{n-1}\right\}$$

$$+ \frac{E\hat{I}_{\phi 2}}{R}\sum_{n=2}^{\infty} n(n-1)g_n x^{n-2} - \frac{E\hat{I}_{23}}{R}\left\{\sum_{n=2}^{\infty} n(n-1)f_n x^{n-2} - \frac{1}{R}\sum_{n=1}^{\infty} nd_n x^{n-1}\right\} - \frac{GA_3}{R}\left(\sum_{n=1}^{\infty} nc_n x^{n-1} + \sum_{n=0}^{\infty} e_n x^n\right)$$

$$-\frac{1}{R}\sum_{n=0}^{\infty}a_n x^n\right) - \frac{GA_{23}}{R}\left(\sum_{n=1}^{\infty}nb_n x^{n-1} - \sum_{n=0}^{\infty}f_n x^n\right) - \frac{GA_{3r}}{R}\left(\sum_{n=1}^{\infty}nd_n x^{n-1} + \sum_{n=0}^{\infty}g_n x^n + \frac{1}{R}\sum_{n=0}^{\infty}f_n x^n\right) \quad (19a)$$

$$-{}^oF_1\left\{\sum_{n=2}^{\infty}n(n-1)a_n x^{n-2} + \frac{2}{R}\sum_{n=1}^{\infty}nc_n x^{n-1} - \frac{1}{R^2}\sum_{n=0}^{\infty}a_n x^n\right\} - {}^oM_2\left\{\sum_{n=2}^{\infty}n(n-1)e_n x^{n-2} - \frac{1}{R}\sum_{n=2}^{\infty}n(n-1)a_n x^{n-2}\right.$$

$$\left. - \frac{2}{R^2}\sum_{n=1}^{\infty}nc_n x^{n-1} - \frac{1}{R^2}\sum_{n=0}^{\infty}e_n x^n + \frac{1}{R^3}\sum_{n=0}^{\infty}a_n x^n\right\} = 0$$

$$GA_2\left\{\sum_{n=2}^{\infty}n(n-1)b_n x^{n-2} - \sum_{n=1}^{\infty}nf_n x^{n-1}\right\} + GA_{23}\left\{\sum_{n=2}^{\infty}n(n-1)c_n x^{n-2} + \sum_{n=1}^{\infty}ne_n x^{n-1} - \frac{1}{R}\sum_{n=1}^{\infty}na_n x^{n-1}\right\}$$

$$+ GA_{2r}\left\{\sum_{n=2}^{\infty}n(n-1)d_n x^{n-2} + \sum_{n=1}^{\infty}ng_n x^{n-1} + \frac{1}{R}\sum_{n=1}^{\infty}nf_n x^{n-1}\right\} - k_y\left(\sum_{n=0}^{\infty}b_n x^n - h_z\sum_{n=0}^{\infty}d_n x^n\right) \quad (19b)$$

$$+ g_y\left\{\sum_{n=2}^{\infty}n(n-1)b_n x^{n-2} - h_z\sum_{n=2}^{\infty}n(n-1)d_n x^{n-2}\right\} + {}^oF_1\sum_{n=2}^{\infty}n(n-1)b_n x^{n-2}$$

$$- {}^oM_2\left\{\sum_{n=2}^{\infty}n(n-1)d_n x^{n-2} + \frac{1}{R}\sum_{n=2}^{\infty}n(n-1)b_n x^{n-2}\right\} = 0$$

$$\frac{EA}{R}\left(\sum_{n=1}^{\infty}na_n x^{n-1} + \frac{1}{R}\sum_{n=0}^{\infty}c_n x^n\right) - \frac{E\hat{I}_2}{R^2}\left(\sum_{n=1}^{\infty}ne_n x^{n-1} - \frac{1}{R}\sum_{n=1}^{\infty}na_n x^{n-1} - \frac{1}{R^2}\sum_{n=0}^{\infty}c_n x^n\right) - \frac{E\hat{I}_{\phi 2}}{R^2}\sum_{n=1}^{\infty}ng_n x^{n-1}$$

$$+ \frac{E\hat{I}_{23}}{R^2}\left(\sum_{n=1}^{\infty}nf_n x^{n-1} - \frac{1}{R}\sum_{n=0}^{\infty}d_n x^n\right) - GA_3\left\{\sum_{n=2}^{\infty}n(n-1)c_n x^{n-2} + \sum_{n=1}^{\infty}ne_n x^{n-1} - \frac{1}{R}\sum_{n=1}^{\infty}na_n x^{n-1}\right\}$$

$$- GA_{23}\left\{\sum_{n=2}^{\infty}n(n-1)b_n x^{n-2} - \sum_{n=1}^{\infty}nf_n x^{n-1}\right\} - GA_{3r}\left\{\sum_{n=2}^{\infty}n(n-1)d_n x^{n-2} + \sum_{n=1}^{\infty}ng_n x^{n-1} + \frac{1}{R}\sum_{n=1}^{\infty}nf_n x^{n-1}\right\} \quad (19c)$$

$$+ k_z\left(\sum_{n=0}^{\infty}c_n x^n + h_y\sum_{n=0}^{\infty}d_n x^n\right) - g_z\left\{\sum_{n=2}^{\infty}n(n-1)c_n x^{n-2} + h_y\sum_{n=2}^{\infty}n(n-1)d_n x^{n-2}\right\}$$

$$+ {}^oF_1\left\{\frac{2}{R}\sum_{n=1}^{\infty}na_n x^{n-1} + \frac{1}{R^2}\sum_{n=0}^{\infty}c_n x^n - \sum_{n=2}^{\infty}n(n-1)c_n x^{n-2}\right\} + {}^oM_2\left\{\frac{2}{R}\sum_{n=1}^{\infty}ne_n x^{n-1} - \frac{2}{R^2}\sum_{n=1}^{\infty}na_n x^{n-1}\right.$$

$$\left. - \frac{1}{R^3}\sum_{n=0}^{\infty}c_n x^n + \frac{1}{R}\sum_{n=2}^{\infty}n(n-1)c_n x^{n-2}\right\} = 0$$

$$-\frac{E\hat{I}_3}{R}\left(\sum_{n=1}^{\infty}nf_n x^{n-1} - \frac{1}{R}\sum_{n=0}^{\infty}d_n x^n\right) + \frac{E\hat{I}_{\phi 3}}{R}\sum_{n=1}^{\infty}ng_n x^{n-1} + \frac{E\hat{I}_{23}}{R}\left(\sum_{n=1}^{\infty}ne_n x^{n-1} - \frac{1}{R}\sum_{n=1}^{\infty}na_n x^{n-1} - \frac{1}{R^2}\sum_{n=0}^{\infty}c_n x^n\right)$$

$$- GJ\left\{\sum_{n=2}^{\infty}n(n-1)d_n x^{n-2} + \frac{1}{R}\sum_{n=1}^{\infty}nf_n x^{n-1}\right\} - GA_r\left\{\sum_{n=2}^{\infty}n(n-1)d_n x^{n-2} + \sum_{n=1}^{\infty}ng_n x^{n-1} + \frac{1}{R}\sum_{n=1}^{\infty}nf_n x^{n-1}\right\}$$

$$- GA_{2r}\left\{\sum_{n=2}^{\infty}n(n-1)b_n x^{n-2} - \sum_{n=1}^{\infty}nf_n x^{n-1}\right\} - GA_{3r}\left\{\sum_{n=2}^{\infty}n(n-1)c_n x^{n-2} + \sum_{n=1}^{\infty}ne_n x^{n-1} - \frac{1}{R}\sum_{n=1}^{\infty}na_n x^{n-1}\right\}$$

$$-k_y h_z \sum_{n=0}^{\infty} b_n x^n + k_z h_y \sum_{n=0}^{\infty} c_n x^n + \left(k_y h_z^2 + k_z h_y^2 + k_\omega\right)\sum_{n=0}^{\infty} d_n x^n + g_y h_z \sum_{n=2}^{\infty} n(n-1)b_n x^{n-2} \tag{19d}$$

$$-g_z h_y \sum_{n=2}^{\infty} n(n-1)c_n x^{n-2} - \left(g_y h_z^2 + g_z h_y^2\right)\sum_{n=2}^{\infty} n(n-1)d_n x^{n-2} - \beta_1 \,{}^o F_1 \left\{ \sum_{n=2}^{\infty} n(n-1)d_n x^{n-2} + \frac{1}{R}\sum_{n=1}^{\infty} n f_n x^{n-1} \right\}$$

$$+\,{}^o M_2 \left\{ \sum_{n=2}^{\infty} n(n-1)b_n x^{n-2} - \frac{1}{R}\sum_{n=0}^{\infty} d_n x^n - \beta_2 \sum_{n=2}^{\infty} n(n-1)d_n x^{n-2} - \frac{\beta_2}{R}\sum_{n=1}^{\infty} n f_n x^{n-1} \right\} = 0$$

$$-E\hat{I}_2 \left\{ \sum_{n=2}^{\infty} n(n-1)e_n x^{n-2} - \frac{1}{R}\sum_{n=2}^{\infty} n(n-1)a_n x^{n-2} - \frac{1}{R^2}\sum_{n=1}^{\infty} n c_n x^{n-1} \right\} - E\hat{I}_{\phi 2} \sum_{n=2}^{\infty} n(n-1)g_n x^{n-2}$$

$$+E\hat{I}_{23} \left\{ \sum_{n=2}^{\infty} n(n-1)f_n x^{n-2} - \frac{1}{R}\sum_{n=1}^{\infty} n d_n x^{n-1} \right\} + GA_3 \left(\sum_{n=1}^{\infty} n c_n x^{n-1} + \sum_{n=0}^{\infty} e_n x^n - \frac{1}{R}\sum_{n=0}^{\infty} a_n x^n \right) \tag{19e}$$

$$+GA_{23} \left(\sum_{n=1}^{\infty} n b_n x^{n-1} - \sum_{n=0}^{\infty} f_n x^n \right) + GA_{3r} \left(\sum_{n=1}^{\infty} n d_n x^{n-1} + \sum_{n=0}^{\infty} g_n x^n + \frac{1}{R}\sum_{n=0}^{\infty} f_n x^n \right)$$

$$+\,{}^o M_2 \left\{ -\sum_{n=2}^{\infty} n(n-1)a_n x^{n-2} - \frac{2}{R}\sum_{n=1}^{\infty} n c_n x^{n-1} - \frac{1}{R}\sum_{n=0}^{\infty} e_n x^n + \frac{1}{R^2}\sum_{n=0}^{\infty} a_n x^n \right\} = 0$$

$$-E\hat{I}_3 \left\{ \sum_{n=2}^{\infty} n(n-1)f_n x^{n-2} - \frac{1}{R}\sum_{n=1}^{\infty} n d_n x^{n-1} \right\} + E\hat{I}_{\phi 3} \sum_{n=2}^{\infty} n(n-1)g_n x^{n-2} + E\hat{I}_{23} \left\{ \sum_{n=2}^{\infty} n(n-1)e_n x^{n-2} \right.$$

$$\left. -\frac{1}{R}\sum_{n=2}^{\infty} n(n-1)a_n x^{n-2} - \frac{1}{R^2}\sum_{n=1}^{\infty} n c_n x^{n-1} \right\} + \frac{GJ}{R}\left(\sum_{n=1}^{\infty} n d_n x^{n-1} + \frac{1}{R}\sum_{n=0}^{\infty} f_n x^n \right) - GA_2 \left(\sum_{n=1}^{\infty} n b_n x^{n-1} - \sum_{n=0}^{\infty} f_n x^n \right)$$

$$-GA_{23} \left(\sum_{n=1}^{\infty} n c_n x^{n-1} + \sum_{n=0}^{\infty} e_n x^n - \frac{1}{R}\sum_{n=0}^{\infty} a_n x^n \right) + \frac{GA_r}{R}\left(\sum_{n=1}^{\infty} n d_n x^{n-1} + \sum_{n=0}^{\infty} g_n x^n + \frac{1}{R}\sum_{n=0}^{\infty} f_n x^n \right) \tag{19f}$$

$$-GA_{2r} \left(\sum_{n=1}^{\infty} n d_n x^{n-1} + \sum_{n=0}^{\infty} g_n x^n - \frac{1}{R}\sum_{n=1}^{\infty} n b_n x^{n-1} + \frac{2}{R}\sum_{n=0}^{\infty} f_n x^n \right) + \frac{GA_{3r}}{R}\left(\sum_{n=1}^{\infty} n c_n x^{n-1} + \sum_{n=0}^{\infty} e_n x^n - \frac{1}{R}\sum_{n=0}^{\infty} a_n x^n \right)$$

$$+\,{}^o F_1 \frac{\beta_1}{R}\left(\sum_{n=1}^{\infty} n d_n x^{n-1} + \frac{1}{R}\sum_{n=0}^{\infty} f_n x^n \right) + \,{}^o M_2 \frac{\beta_2}{R}\left(\sum_{n=1}^{\infty} n d_n x^{n-1} + \frac{1}{R}\sum_{n=0}^{\infty} f_n x^n \right) = 0$$

$$-E\hat{I}_\phi \sum_{n=2}^{\infty} n(n-1)g_n x^{n-2} - E\hat{I}_{\phi 2} \left\{ \sum_{n=2}^{\infty} n(n-1)e_n x^{n-2} - \frac{1}{R}\sum_{n=2}^{\infty} n(n-1)a_n x^{n-2} - \frac{1}{R^2}\sum_{n=1}^{\infty} n c_n x^{n-1} \right\}$$

$$+E\hat{I}_{\phi 3} \left\{ \sum_{n=2}^{\infty} n(n-1)f_n x^{n-2} - \frac{1}{R}\sum_{n=1}^{\infty} n d_n x^{n-1} \right\} + GA_r \left(\sum_{n=1}^{\infty} n d_n x^{n-1} + \sum_{n=0}^{\infty} g_n x^n + \frac{1}{R}\sum_{n=0}^{\infty} f_n x^n \right) \tag{19g}$$

$$+GA_{2r} \left(\sum_{n=1}^{\infty} n b_n x^{n-1} - \sum_{n=0}^{\infty} f_n x^n \right) + GA_{3r} \left(\sum_{n=1}^{\infty} n c_n x^{n-1} + \sum_{n=0}^{\infty} e_n x^n - \frac{1}{R}\sum_{n=0}^{\infty} a_n x^n \right) = 0$$

By shifting the index of power of x^n in Eqs. 19(a-g) and rearranging equations, the following equations can be obtained.

$$\sum_{n=0}^{\infty}\left[-EA(n+2)(n+1)a_{n+2}-\frac{EA}{R}(n+1)c_{n+1}+\frac{E\hat{I}_{2}}{R}(n+2)(n+1)e_{n+2}-\frac{E\hat{I}_{2}}{R^{2}}(n+2)(n+1)a_{n+2}\right.$$

$$-\frac{E\hat{I}_{2}}{R^{3}}(n+1)c_{n+1}+\frac{E\hat{I}_{\phi2}}{R}(n+2)(n+1)g_{n+2}-\frac{E\hat{I}_{23}}{R}(n+2)(n+1)f_{n+2}+\frac{E\hat{I}_{23}}{R^{2}}(n+1)d_{n+1}-\frac{GA_{3}}{R}e_{n}$$

$$-\frac{GA_{3}}{R}(n+1)c_{n+1}+\frac{GA_{3}}{R^{2}}a_{n}-\frac{GA_{23}}{R}(n+1)b_{n+1}+\frac{GA_{23}}{R}f_{n}-\frac{GA_{3r}}{R}(n+1)d_{n+1}-\frac{GA_{3r}}{R}g_{n}-\frac{GA_{3r}}{R^{2}}f_{n}\quad(20a)$$

$$-{}^{o}F_{1}\left\{(n+2)(n+1)a_{n+2}+\frac{2}{R}(n+1)c_{n+1}-\frac{1}{R^{2}}a_{n}\right\}-{}^{o}M_{2}\left\{(n+2)(n+1)e_{n+2}-\frac{1}{R}(n+2)(n+1)a_{n+2}\right.$$

$$\left.\left.-\frac{2}{R^{2}}(n+1)c_{n+1}-\frac{1}{R^{2}}e_{n}+\frac{1}{R^{3}}a_{n}\right\}\right]=0$$

$$\sum_{n=0}^{\infty}\left[GA_{2}(n+2)(n+1)b_{n+2}-GA_{2}(n+1)f_{n+1}+GA_{23}(n+2)(n+1)c_{n+2}+GA_{23}(n+1)e_{n+1}\right.$$

$$-\frac{GA_{23}}{R}(n+1)a_{n+1}+GA_{2r}(n+2)(n+1)d_{n+2}+GA_{2r}(n+1)g_{n+1}+\frac{GA_{2r}}{R}(n+1)f_{n+1}\quad(20b)$$

$$-k_{y}b_{n}+k_{y}h_{z}d_{n}+g_{y}(n+2)(n+1)b_{n+2}-g_{y}h_{z}(n+2)(n+1)d_{n+2}$$

$$\left.+{}^{o}F_{1}(n+2)(n+1)b_{n+2}-{}^{o}M_{2}\left\{\frac{1}{R}(n+2)(n+1)b_{n+2}+(n+2)(n+1)d_{n+2}\right\}\right]=0$$

$$\sum_{n=0}^{\infty}\left[\frac{EA}{R}(n+1)a_{n+1}+\frac{EA}{R^{2}}c_{n}-\frac{E\hat{I}_{2}}{R^{2}}(n+1)e_{n+1}+\frac{E\hat{I}_{2}}{R^{3}}(n+1)a_{n+1}+\frac{E\hat{I}_{2}}{R^{4}}c_{n}-\frac{E\hat{I}_{\phi2}}{R^{2}}(n+1)g_{n+1}\right.$$

$$+\frac{E\hat{I}_{23}}{R^{2}}(n+1)f_{n+1}-\frac{E\hat{I}_{23}}{R^{3}}d_{n}-GA_{3}(n+2)(n+1)c_{n+2}-GA_{3}(n+1)e_{n+1}+\frac{GA_{3}}{R}(n+1)a_{n+1}$$

$$-GA_{23}(n+2)(n+1)b_{n+2}+GA_{23}(n+1)f_{n+1}-GA_{3r}(n+2)(n+1)d_{n+2}-GA_{3r}(n+1)g_{n+1}$$

$$-\frac{GA_{3r}}{R}(n+1)f_{n+1}+k_{z}c_{n}+k_{z}h_{y}d_{n}-g_{z}(n+2)(n+1)c_{n+2}-g_{z}h_{y}(n+2)(n+1)d_{n+2}\quad(20c)$$

$$+{}^{o}F_{1}\left\{\frac{2}{R}(n+1)a_{n+1}+\frac{1}{R^{2}}c_{n}-(n+2)(n+1)c_{n+2}\right\}+{}^{o}M_{2}\left\{\frac{2}{R}(n+1)e_{n+1}-\frac{2}{R^{2}}(n+1)a_{n+1}\right.$$

$$\left.\left.-\frac{1}{R^{3}}c_{n}+\frac{1}{R}(n+2)(n+1)c_{n+2}\right\}\right]=0$$

$$\sum_{n=0}^{\infty}\left[-\frac{E\hat{I}_{3}}{R}(n+1)f_{n+1}+\frac{E\hat{I}_{3}}{R^{2}}d_{n}+\frac{E\hat{I}_{\phi3}}{R}(n+1)g_{n+1}+\frac{E\hat{I}_{23}}{R}(n+1)e_{n+1}-\frac{E\hat{I}_{23}}{R^{2}}(n+1)a_{n+1}-\frac{E\hat{I}_{23}}{R^{3}}c_{n}\right.$$

$$-GJ(n+2)(n+1)d_{n+2}-\frac{GJ}{R}(n+1)f_{n+1}-GA_{r}(n+2)(n+1)d_{n+2}-GA_{r}(n+1)g_{n+1}-\frac{GA_{r}}{R}(n+1)f_{n+1}$$

$$-GA_{2r}(n+2)(n+1)b_{n+2} + GA_{2r}(n+1)f_{n+1} - GA_{3r}(n+2)(n+1)c_{n+2} - GA_{3r}(n+1)e_{n+1} + \frac{GA_{3r}}{R}(n+1)a_{n+1}$$

$$-k_y h_z b_n + k_z h_y c_n + \left(k_y h_z^2 + k_z h_y^2 + k_\omega\right)d_n + g_y h_z(n+2)(n+1)b_{n+2} - g_z h_y(n+2)(n+1)c_{n+2} \quad (20d)$$

$$-\left(g_y h_z^2 + g_z h_y^2\right)(n+2)(n+1)d_{n+2} - \beta_1{}^oF_1\left\{(n+2)(n+1)d_{n+2} + \frac{1}{R}(n+1)f_{n+1}\right\}$$

$$+{}^oM_2\left\{-\frac{1}{R}d_n + (n+2)(n+1)b_{n+2} - \beta_2(n+2)(n+1)d_{n+2} - \frac{\beta_2}{R}(n+1)f_{n+1}\right\}\Bigg] = 0$$

$$\sum_{n=0}^{\infty}\Bigg[-E\hat{I}_2(n+2)(n+1)e_{n+2} + \frac{E\hat{I}_2}{R}(n+2)(n+1)a_{n+2} + \frac{E\hat{I}_2}{R^2}(n+1)c_{n+1} - E\hat{I}_{\phi2}(n+2)(n+1)g_{n+2}$$

$$+E\hat{I}_{23}(n+2)(n+1)f_{n+2} - \frac{E\hat{I}_{23}}{R}(n+1)d_{n+1} + GA_3(n+1)c_{n+1} + GA_3 e_n - \frac{GA_3}{R}a_n + GA_{23}(n+1)b_{n+1}$$

$$-GA_{23}f_n + GA_{3r}(n+1)d_{n+1} + GA_{3r}g_n + \frac{GA_{3r}}{R}f_n \quad (20e)$$

$$^oM_2\left\{-(n+2)(n+1)a_{n+2} - \frac{2}{R}(n+1)c_{n+1} - \frac{1}{R}e_n + \frac{1}{R^2}e_n\right\}\Bigg] = 0$$

$$\sum_{n=0}^{\infty}\Bigg[-E\hat{I}_3(n+2)(n+1)f_{n+2} + \frac{E\hat{I}_3}{R}(n+1)d_{n+1} + E\hat{I}_{\phi3}(n+2)(n+1)g_{n+2} + E\hat{I}_{23}(n+2)(n+1)e_{n+2}$$

$$-\frac{E\hat{I}_{23}}{R}(n+2)(n+1)a_{n+2} - \frac{E\hat{I}_{23}}{R^2}(n+1)c_{n+1} + \frac{GJ}{R}(n+1)d_{n+1} + \frac{GJ}{R^2}f_n - GA_2(n+1)b_{n+1} + GA_2 f_n$$

$$-GA_{23}(n+1)c_{n+1} - GA_{23}e_n + \frac{GA_{23}}{R}a_n + \frac{GA_r}{R}(n+1)d_{n+1} + \frac{GA_r}{R}g_n + \frac{GA_r}{R^2}f_n - GA_{2r}(n+1)d_{n+1} \quad (20f)$$

$$-GA_{2r}g_n + \frac{GA_{2r}}{R}(n+1)b_{n+1} - \frac{2}{R}GA_{2r}f_n + \frac{GA_{3r}}{R}(n+1)c_{n+1} + \frac{GA_{3r}}{R}e_n - \frac{GA_{3r}}{R^2}a_n$$

$$+{}^oF_1\frac{\beta_1}{R}\left\{(n+1)d_{n+1} + \frac{1}{R}f_n\right\} + {}^oM_2\frac{\beta_2}{R}\left\{(n+1)d_{n+1} + \frac{1}{R}f_n\right\}\Bigg] = 0$$

$$\sum_{n=0}^{\infty}\Bigg[-E\hat{I}_\phi(n+2)(n+1)g_{n+2} - E\hat{I}_{\phi2}(n+2)(n+1)e_{n+2} + \frac{E\hat{I}_{\phi2}}{R}(n+2)(n+1)a_{n+2} + \frac{E\hat{I}_{\phi2}}{R^2}(n+1)c_{n+1}$$

$$+E\hat{I}_{\phi3}(n+2)(n+1)f_{n+2} - \frac{E\hat{I}_{\phi3}}{R}(n+1)d_{n+1} + GA_r(n+1)d_{n+1} + GA_r g_n + \frac{GA_r}{R}f_n + GA_{2r}(n+1)b_{n+1} \quad (20g)$$

$$-GA_{2r}f_n + GA_{3r}(n+1)c_{n+1} + GA_{3r}e_n - \frac{GA_{3r}}{R}a_n\Bigg] = 0$$

Eqs. (20a-g) can be compactly expressed in a matrix form as follows

$$\sum_{n=0}^{\infty} \mathbf{A_n} \{a_{n+2}, b_{n+2}, c_{n+2}, d_{n+2}, e_{n+2}, f_{n+2}, g_{n+2}\}^T$$

$$= \sum_{n=0}^{\infty} \mathbf{B_n} \{a_n, a_{n+1}, b_n, b_{n+1}, c_n, c_{n+1}, d_n, d_{n+1}, e_n, e_{n+1}, f_n, f_{n+1}, g_n, g_{n+1}\}^T \tag{21}$$

where the detailed expressions for matrices $\mathbf{A_n}$ and $\mathbf{B_n}$ are given in Appendix A. Eq. (21) can be rewritten as

$$\sum_{n=0}^{\infty} \{a_{n+2}, b_{n+2}, c_{n+2}, d_{n+2}, e_{n+2}, f_{n+2}, g_{n+2}\}^T$$

$$= \sum_{n=0}^{\infty} \mathbf{Z_n} \{a_n, a_{n+1}, b_n, b_{n+1}, c_n, c_{n+1}, d_n, d_{n+1}, e_n, e_{n+1}, f_n, f_{n+1}, g_n, g_{n+1}\}^T \tag{22}$$

where

$$\mathbf{Z_n} = \mathbf{A_n^{-1}} \mathbf{B_n} \tag{23}$$

In case of $n = 0$, 1, and i ($i \geq 2$), we can obtain the following relations from Eq. (22).
For $n = 0$;

$$\{a_2, b_2, c_2, d_2, e_2, f_2, g_2\}^T$$

$$= \mathbf{Z_0} \{a_0, a_1, b_0, b_1, c_0, c_1, d_0, d_1, e_0, e_1, f_0, f_1, g_0, g_1\}^T \tag{24}$$

$$= \mathbf{L_2} \mathbf{a}$$

For $n = 1$;

$$\{a_3, b_3, c_3, d_3, e_3, f_3, g_3\}^T$$

$$= \mathbf{Z_1} \{a_1, a_2, b_1, b_2, c_1, c_2, d_1, d_2, e_1, e_2, f_1, f_2, g_1, g_2\}^T$$

$$= \mathbf{Z_1} \cdot \mathbf{N_1} \{a_0, a_1, b_0, b_1, c_0, c_1, d_0, d_1, e_0, e_1, f_0, f_1, g_0, g_1\}^T \tag{25}$$

$$= \mathbf{L_3} \mathbf{a}$$

For $n = i$ ($i \geq 2$);

$$\{a_{i+2}, b_{i+2}, c_{i+2}, d_{i+2}, e_{i+2}, f_{i+2}, g_{i+2}\}$$

$$= \mathbf{Z_i} \cdot \mathbf{N_i} \{a_i, a_{i+1}, b_i, b_{i+1}, c_i, c_{i+1}, d_i, d_{i+1}, e_i, e_{i+1}, f_i, f_{i+1}, g_i, g_{i+1}\}^T \tag{26}$$

$$= \mathbf{L_{i+2}} \mathbf{a}$$

where the matrices $\mathbf{N_1}$ and $\mathbf{N_i}$ are presented in Appendix B and $\mathbf{a}$ denotes the initial integration constant vector defined by

$$\mathbf{a} = \{a_0, a_1, b_0, b_1, c_0, c_1, d_0, d_1, e_0, e_1, f_0, f_1, g_0, g_1\}^T \tag{27}$$

By substituting the integration constant vector obtained by Eq. (26) into Eq. (18) and rearranging Eq. (17), the displacement state vector composed of 14 displacement parameters in Eq. (17) is expressed with respect to the initial integration constant vector $\mathbf{a}$ as follows

$$\mathbf{d} = \mathbf{X_n} \mathbf{a} \tag{28}$$

In each of these 14 solution sets, the calculation of the coefficients by the recursive relations in Eq. (24) through Eq. (26) is continued until the contribution of the next coefficient is less than an arbitrarily chosen small number. In this study, above symbolic calculations are performed with the help of the technical computer software Methematica (Wolfram 2005).

Next, the initial integration constant vector $\mathbf{a}$ can be expressed with respect to 14 nodal displacement components. For this, we consider the nodal displacement vector at p and q which mean the two ends of the curved member $(x_1 = 0, l)$ is defined by

$$\mathbf{U}_e = <\mathbf{U}^p, \mathbf{U}^q>^T \tag{29}$$

where

$$\mathbf{U}^p = <U_x(0), U_y(0), U_z(0), \omega_1(0), \omega_2(0), \omega_3(0), f(0)>^T \tag{30a}$$

$$\mathbf{U}^q = <U_x(l), U_y(l), U_z(l), \omega_1(l), \omega_2(l), \omega_3(l), f(l)>^T \tag{30b}$$

Substituting coordinates of the ends of member $(x_1 = 0, l)$ into Eq. (28), the nodal displacement vector $\mathbf{U}_e$ is expressed as follows

$$\mathbf{U}_e = \mathbf{H}\mathbf{a} \tag{31}$$

Elimination of $\mathbf{a}$ from Eq. (28) using Eq. (31) yields the displacement state vector consisting of 14 displacement components.

$$\mathbf{d} = \mathbf{X}_n \mathbf{H}^{-1} \mathbf{U}_e \tag{32}$$

3.1.2 Calculation of stiffness matrix

In order to calculate the element stiffness matrix of curved beam based on the displacement function derived in this study, we consider the nodal force vector at two ends p and q defined by

$$\mathbf{F}_e = <\mathbf{F}^p, \mathbf{F}^q>^T \tag{33}$$

where

$$\mathbf{F}^\xi = <F_1^\xi, F_2^\xi, F_3^\xi, M_1^\xi, M_2^\xi, M_3^\xi, M_\phi^\xi>^T, \quad \xi = p, q \tag{34}$$

The force-deformation relations in Eqs. (16a-g) can be expressed in a matrix form as follows

$$\mathbf{f} = \mathbf{S}\mathbf{d} \tag{35}$$

where each components of 7×14 matrix $\mathbf{S}$ is given in Appendix A.

Substitution of the displacement function in Eq. (32) into Eq. (35) leads to

$$\mathbf{f} = \mathbf{S}\mathbf{X}_n \mathbf{H}^{-1} \mathbf{U}_e \tag{36}$$

And nodal forces at ends of the curved element are evaluated as

$$\mathbf{F}^p = -\mathbf{f}(0) = -\mathbf{S}\mathbf{X}_n(0)\mathbf{H}^{-1}\mathbf{U}_e \tag{37a}$$

$$\mathbf{F}^q = \mathbf{f}(l) = \mathbf{S}\mathbf{X}_n(l)\mathbf{H}^{-1}\mathbf{U}_e \tag{37b}$$

Consequently the element stiffness matrix of thin-walled Timoshenko curved beam with non-symmetric cross-section resting on elastic foundation is evaluated as

$$\mathbf{F}_e = \mathbf{K}\mathbf{U}_e \tag{38}$$

where

$$\mathbf{K} = \begin{bmatrix} -\mathbf{SX_n}(0)\mathbf{H}^{-1} \\ \mathbf{SX_n}(l)\mathbf{H}^{-1} \end{bmatrix} \tag{39}$$

The buckling loads and moments are the values that cause the stiffness matrix for the element to become singular. In this study, the Regular-Falsi method (Wendroff 1966) is applied to ensure that none of buckling loads and moments is missed. It can be noted that the stiffness matrix in Eq. (39) is formed by the shape functions which are solutions of the equilibrium equations. Therefore, the accurate curved beam element based on the stiffness matrix developed by this study eliminates discretization errors and is free from the shear locking. In addition, the buckling mode shapes can be calculated from Eq. (18) and Eqs. (24) to (26).

3.2 Stiffness matrix for in-plane buckling of curved beam subjected to uniform compression

As a special case, we present the element stiffness matrix for in-plane buckling analysis of curved beam with double- and mono-symmetric cross-sections subjected to uniform compression $^{o}F_1$. It is known that the in-plane and out-of-plane buckling modes of this curved beam are decoupled because the section is symmetric in the plane of beam curvature. Therefore, the total potential energy corresponding to in-plane bucking mode is given from Eq. (14) as follows

$$\Pi_{in} = \frac{1}{2}\int_{o}^{l}\left[EA\left(U_x' + \frac{U_z}{R}\right)^2 + E\hat{I}_2\left(\omega_2' - \frac{U_x'}{R} - \frac{U_z}{R^2}\right)^2 + GA_3\left(U_z' - \frac{U_x}{R} + \omega_2\right)^2\right.$$

$$\left. + k_z U_z^2 + g_z U_z'^2 + {}^{o}F_1\left\{\left(U_x' + \frac{U_z}{R}\right)^2 + \left(U_z' - \frac{U_x}{R}\right)^2\right\}\right]dx_1 \tag{40}$$

From the stationary condition, the equilibrium equations and force-deformation relations are obtained as follows

$$-EA\left(U_x'' + \frac{U_z'}{R}\right)^2 + \frac{1}{R}E\hat{I}_2\left(\omega_2'' - \frac{U_x''}{R} - \frac{U_z'}{R^2}\right) - \frac{1}{R}GA_3\left(U_z' + \omega_2 - \frac{U_x}{R}\right)$$

$$-{}^{o}F_1\left\{\left(U_x'' + \frac{U_z'}{R}\right) + \frac{1}{R}\left(U_z' - \frac{U_x}{R}\right)\right\} = 0 \tag{41a}$$

$$\frac{1}{R}EA\left(U_x' + \frac{U_z}{R}\right) - \frac{1}{R^2}E\hat{I}_2\left(\omega_2' - \frac{U_x'}{R} - \frac{U_z}{R^2}\right) - GA_3\left(U_z'' + \omega_2' - \frac{U_x'}{R}\right) + k_z U_z - g_z U_z''$$

$$+ {}^{o}F_1\left\{\frac{1}{R}\left(U_x' + \frac{U_z}{R}\right) - \left(U_z'' - \frac{U_x'}{R}\right)\right\} = 0 \tag{41b}$$

$$-E\hat{I}_2\left(\omega_2'' - \frac{1}{R}U_x'' - \frac{1}{R^2}U_z'\right) + GA_3\left(U_z' + \omega_2 - \frac{1}{R}U_x\right) = 0 \tag{41c}$$

The force-deformation relations corresponding to the in-plane buckling mode are

$$F_1^{in} = EA\left(U_x' + \frac{U_z}{R}\right) - \frac{1}{R}E\hat{I}_2\left(\omega_2' - \frac{U_x'}{R} - \frac{U_z}{R^2}\right) + {}^oF_1\left(U_x' + \frac{U_z}{R}\right) \tag{42a}$$

$$F_3^{in} = GA_3\left(U_z' + \omega_2 - \frac{U_x}{R}\right) + g_z U_z' + {}^oF_1\left(U_z' - \frac{U_x}{R}\right) \tag{42b}$$

$$M_2^{in} = E\hat{I}_2\left(\omega_2' - \frac{U_x'}{R} - \frac{U_z}{R^2}\right) \tag{42c}$$

By substituting the displacement parameters U_x, U_z, and ω_2 as the infinite power series forms in Eqs. (18a), (18c), and (18e) into the equilibrium equations in Eqs. (41a-c), the following polynomial expansions of those equations are obtained.

$$\sum_{n=0}^{\infty}\left[-EA(n+2)(n+1)a_{n+2} - \frac{EA}{R}(n+1)c_{n+1} + \frac{E\hat{I}_2}{R}(n+2)(n+1)e_{n+2}\right.$$

$$-\frac{E\hat{I}_2}{R}(n+2)(n+1)a_{n+2} - \frac{E\hat{I}_2}{R^3}(n+1)c_{n+1} - \frac{GA_3}{R}e_n - \frac{GA_3}{R}(n+1)c_{n+1} + \frac{GA_3}{R^2}a_n \tag{43a}$$

$$\left. -{}^oF_1\left\{(n+2)(n+1)a_{n+2} + \frac{2}{R}(n+1)c_{n+1} - \frac{1}{R^2}a_n\right\}\right] = 0$$

$$\sum_{n=0}^{\infty}\left[\frac{EA}{R}(n+1)a_{n+1} + \frac{EA}{R^2}c_n - \frac{E\hat{I}_2}{R^2}(n+1)e_{n+1} + \frac{E\hat{I}_2}{R^3}(n+1)a_{n+1} + \frac{E\hat{I}_2}{R^4}c_n\right.$$

$$- GA_3(n+2)(n+1)c_{n+2} - GA_3(n+1)e_{n+1} + \frac{GA_3}{R}(n+1)a_{n+1} + k_z c_n \tag{43b}$$

$$\left. -g_z(n+2)(n+1)c_{n+2} + {}^oF_1\left\{\frac{2}{R}(n+1)a_{n+1} + \frac{1}{R^2}c_n - (n+2)(n+1)c_{n+2}\right\}\right] = 0$$

$$\sum_{n=0}^{\infty}\left[-E\hat{I}_2(n+2)(n+1)e_{n+2} + \frac{E\hat{I}_2}{R}(n+2)(n+1)a_{n+2} + \frac{E\hat{I}_2}{R^2}(n+1)c_{n+1}\right.$$

$$\left. + GA_3(n+1)c_{n+1} + GA_3 e_n - \frac{GA_3}{R}a_n\right] = 0 \tag{43c}$$

These equations may be expressed in a matrix form as

$$\sum_{n=0}^{\infty}\{a_{n+2}, c_{n+2}, e_{n+2}\}^T = \sum_{n=0}^{\infty}\mathbf{Z_n^{in}}\{a_n, a_{n+1}, c_n, c_{n+1}, e_n, e_{n+1}\}^T \tag{44}$$

where

$$\mathbf{Z_n^{in}} = \mathbf{A_n^{in^{-1}}}\mathbf{B_n^{in}} \tag{45}$$

The detailed expressions for matrices $\mathbf{A_n^{in}}$ and $\mathbf{B_n^{in}}$ corresponding to in-plane buckling mode are

presented in Appendix C. Then, the displacement function matrix is derived using the relations between the nodal displacement vector $\mathbf{U}_e^{in}$ and the initial constant vector $\mathbf{a}^{in}$. Finally, the element stiffness matrix of the curved beam for in-plane buckling analysis can be derived from the relations between the nodal forces and the nodal displacements at two ends of the beam as follows:

$$\mathbf{F}_e^{in} = \mathbf{K}^{in}\mathbf{U}_e^{in} \tag{46}$$

where

$$\mathbf{K}^{in} = \begin{bmatrix} -\mathbf{S}^{in}\mathbf{X}_n^{in}(0)\mathbf{H}^{in^{-1}} \\ \mathbf{S}^{in}\mathbf{X}_n^{in}(l)\mathbf{H}^{in^{-1}} \end{bmatrix} \tag{47}$$

3.3 Stiffness matrix for out-of-plane buckling of curved beam subjected to uniform compression and pure bending

We consider lateral-torsional buckling of the double- and mono-symmetric thin-walled curved beam subjected to uniform compression $^oF_1$ and pure bending $^oM_2$. The total potential energy corresponding to out-of-plane buckling mode is given as follows

$$\begin{aligned}
\Pi_{out} &= \frac{1}{2}\int_o^l \left[E\hat{I}_3\left(\omega_3' - \frac{\omega_1}{R}\right)^2 + E\hat{I}_\phi f'^2 - 2E\hat{I}_{\phi 3}\left(\omega_3' - \frac{\omega_1}{R}\right)f' + GJ\left(\omega_1' + \frac{\omega_3}{R}\right)^2 \right. \\
&\quad + GA_2\left(U_y' - \omega_3\right)^2 + GA_r\left(\omega_1' + \frac{\omega_3}{R} + f\right)^2 + 2GA_{2r}\left(U_y' - \omega_3\right)\left(\omega_1' + \frac{\omega_3}{R} + f\right) \\
&\quad + k_y\left(U_y - h_z\omega_1\right)^2 + k_z h_y^2\omega_1^2 + k_\omega\omega_1^2 + g_y\left(U_y' - h_z\omega_1'\right)^2 + g_z h_y^2\omega_1'^2 \\
&\quad \left. +^oF_1 U_y'^2 +^oM_2\left\{\omega_1'\omega_3 + \omega_1\omega_3' - \frac{1}{R}\left(U_y'^2 + \omega_1^2\right) - 2U_y'\omega'\right\} + \left(\beta_1{}^oF_1 + \beta_2{}^oM_2\right)\left(\omega_1' + \frac{\omega_3}{R}\right)^2 \right]dx_1
\end{aligned} \tag{48}$$

The equilibrium equations and force-deformation relations corresponding to out-of-plane deformation mode are derived from the stationary condition as follows

$$\begin{aligned}
&GA_2\left(U_y'' - \omega_3'\right) + GA_{2r}\left(\omega_1'' + f' + \frac{\omega_3'}{R}\right) - k_y\left(U_y - h_z\omega_1\right) + g_y\left(U_y'' - h_z\omega_1''\right) \\
&\quad +^oF_1 U_y'' -^oM_2\left(\omega_1'' + \frac{U_y''}{R}\right) = 0
\end{aligned} \tag{49a}$$

$$\begin{aligned}
&-\frac{1}{R}E\hat{I}_3\left(\omega_3' - \frac{\omega_1}{R}\right) + \frac{1}{R}E\hat{I}_{\phi 3}f' - GJ\left(\omega_1'' + \frac{\omega_3'}{R}\right) - GA_r\left(\omega_1'' + f' + \frac{\omega_3'}{R}\right) \\
&- GA_{2r}\left(U_y'' - \omega_3'\right) - k_y h_z U_y + \left(k_y h_z^2 + k_z h_y^2 + k_\omega\right)\omega_1 + g_y h_z U_y'' - \left(g_y h_z^2 + g_z h_y^2\right)\omega_1'' \\
&\quad -\beta_1{}^oF_1\left(\omega_1'' + \frac{\omega_3'}{R}\right) +^oM_2\left\{U_y'' - \frac{\omega_1}{R} - \beta_2\left(\omega_1'' + \frac{\omega_3'}{R}\right)\right\} = 0
\end{aligned} \tag{49b}$$

$$-E\hat{I}_3\left(\omega_3''-\frac{1}{R}\omega_1'\right)+E\hat{I}_{\phi3}f''+\frac{1}{R}GJ\left(\omega_1'+\frac{1}{R}\omega_3\right)-GA_2\left(U_y'-\omega_3\right)+\frac{1}{R}GA_r\left(\omega_1'+f+\frac{1}{R}\omega_3\right)$$

$$-GA_{2r}\left(\omega_1'+f-\frac{1}{R}U_y'+\frac{2}{R}\omega_3\right)+{}^oF_1\frac{\beta_1}{R}\left(\omega_1'+\frac{\omega_3}{R}\right)+{}^oM_2\frac{\beta_2}{R}\left(\omega_1'+\frac{\omega_3}{R}\right)=0 \tag{49c}$$

$$-E\hat{I}_\phi f''+E\hat{I}_{\phi3}\left(\omega_3''-\frac{1}{R}\omega_1'\right)+GA_r\left(\omega_1'+f+\frac{1}{R}\omega_3\right)+GA_{2r}\left(U_y'-\omega_3\right)=0 \tag{49d}$$

Substitution of the Eqs. (18b), (18d), (18f), and (18g) into Eqs. (49a-d) leads to the following polynomial expansions of the equilibrium equations.

$$\sum_{n=0}^{\infty}\Big[GA_2(n+2)(n+1)b_{n+2}-GA_2(n+1)f_{n+1}+GA_{2r}(n+2)(n+1)d_{n+2}+GA_{2r}(n+1)g_{n+1}$$

$$+\frac{GA_{2r}}{R}(n+1)f_{n+1}-k_yb_n+k_yh_zd_n+g_y(n+2)(n+1)b_{n+2}-g_yh_z(n+2)(n+1)d_{n+2} \tag{50a}$$

$$+{}^oF_1(n+2)(n+1)b_{n+2}-{}^oM_2\left\{\frac{1}{R}(n+2)(n+1)b_{n+2}+(n+2)(n+1)d_{n+2}\right\}\Big]=0$$

$$\sum_{n=0}^{\infty}\Big[-\frac{E\hat{I}_3}{R}(n+1)f_{n+1}+\frac{E\hat{I}_3}{R^2}d_n+\frac{E\hat{I}_{\phi3}}{R}(n+1)g_{n+1}-GJ(n+2)(n+1)d_{n+2}-\frac{GJ}{R}(n+1)f_{n+1}$$

$$-GA_r(n+2)(n+1)d_{n+2}-GA_r(n+1)g_{n+1}-\frac{GA_r}{R}(n+1)f_{n+1}-GA_{2r}(n+2)(n+1)b_{n+2}$$

$$+GA_{2r}(n+1)f_{n+1}-k_yh_zb_n+\left(k_yh_z^2+k_zh_y^2+k_\omega\right)d_n+g_yh_z(n+2)(n+1)b_{n+2} \tag{50b}$$

$$-\left(g_yh_z^2+g_zh_y^2\right)(n+2)(n+1)d_{n+2}-\beta_1{}^oF_1\left\{(n+2)(n+1)d_{n+2}+\frac{1}{R}(n+1)f_{n+1}\right\}$$

$$+{}^oM_2\left\{(n+2)(n+1)b_{n+2}-\frac{1}{R}d_n-\beta_2(n+2)(n+1)d_{n+2}-\frac{\beta_2}{R}(n+1)f_{n+1}\right\}\Big]=0$$

$$\sum_{n=0}^{\infty}\Big[-E\hat{I}_3(n+2)(n+1)f_{n+2}+\frac{E\hat{I}_3}{R}(n+1)d_{n+1}+E\hat{I}_{\phi3}(n+2)(n+1)g_{n+2}+\frac{GJ}{R}(n+1)d_{n+1}+\frac{GJ}{R^2}f_n$$

$$-GA_2(n+1)b_{n+1}+GA_2f_n+\frac{GA_r}{R}(n+1)d_{n+1}+\frac{GA_r}{R}g_n+\frac{GA_r}{R^2}f_n-GA_{2r}(n+1)d_{n+1}-GA_{2r}g_n \tag{50c}$$

$$+\frac{GA_{2r}}{R}(n+1)b_{n+1}-\frac{2}{R}GA_{2r}f_n+{}^oF_1\frac{\beta_1}{R}\left\{(n+1)d_{n+1}+\frac{1}{R}f_n\right\}+{}^oM_2\frac{\beta_2}{R}\left\{(n+1)d_{n+1}+\frac{1}{R}f_n\right\}\Big]=0$$

$$\sum_{n=0}^{\infty}\Big[-E\hat{I}_\phi(n+2)(n+1)g_{n+2}+E\hat{I}_{\phi3}(n+2)(n+1)f_{n+2}-\frac{E\hat{I}_{\phi3}}{R}(n+1)d_{n+1}+GA_r(n+1)d_{n+1}$$

$$+GA_rg_n+\frac{GA_r}{R}f_n+GA_{2r}(n+1)b_{n+1}-GA_{2r}f_n\Big]=0 \tag{50d}$$

Eqs. (50a-d) can also be compactly expressed as follows:

$$\sum_{n=0}^{\infty}\{b_{n+2},\ d_{n+2},\ f_{n+2},\ g_{n+2}\}^T=\sum_{n=0}^{\infty}\mathbf{Z_n^{out}}\{b_n,\ b_{n+1},\ d_n,\ d_{n+1},\ f_n,\ f_{n+1},\ g_n,\ g_{n+1}\}^T \tag{51}$$

where

$$\mathbf{Z_n^{out}} = \mathbf{A_n^{out^{-1}}} \mathbf{B_n^{out}} \tag{52}$$

The expressions for matrices $\mathbf{A_n^{out}}$ and $\mathbf{B_n^{out}}$ corresponding to out-of-plane buckling mode are presented in Appendix D and the evaluated element stiffness matrix of the curved beam for the lateral-torsional buckling analysis is as follows

$$\mathbf{K^{out}} = \begin{bmatrix} -\mathbf{S^{out}}\mathbf{X_n^{out}}(0)\mathbf{H^{out^{-1}}} \\ \mathbf{S^{out}}\mathbf{X_n^{out}}(l)\mathbf{H^{out^{-1}}} \end{bmatrix} \tag{53}$$

4. Finite element formulation

For comparison, the finite element formulation based on the classical isoparametric curved beam elements having the thin-walled cross-section and the shear deformations is presented. In this study, the 3-noded isoparametric curved beam element with 7 DOF per node is introduced to interpolate displacement parameters that are defined at centroid. The coordinate and all the displacement parameters of the beam element can be interpolated with respect to the nodal coordinates and displacements, respectively, as follows

$$x_1 = \frac{l}{2}(1 + r) \tag{54a}$$

$$U_i = \sum_{\eta = 1}^{3} R_\eta(r)U_i^\eta \quad i = x, y, z \tag{54b}$$

$$\omega_i = \sum_{\eta = 1}^{3} R_\eta(r)\omega_i^\eta \quad i = 1, 2, 3 \tag{54c}$$

$$f = \sum_{\eta = 1}^{3} R_\eta(r)f^\eta \tag{54d}$$

where U_i^η, ω_i^η, and f^η are the translational and rotational displacements in the x_i direction and warping parameter at node η, respectively; R_η is the Lagrangian interpolation function whose detailed expression is presented in Bathe (1996); r is a natural coordinate that varies from -1 to $+1$.

The element displacement vector $\mathbf{U}_{fe}$ and force vector $\mathbf{F}_{fe}$ for the isoparametric curved beam element are defined as

$$\mathbf{U}_{fe} = [U^1, U^2, U^3] \tag{55a}$$

$$\mathbf{U}^\eta = [U_x^\eta, U_y^\eta, U_z^\eta, \omega_1^\eta, \omega_2^\eta, \omega_3^\eta, f^\eta]^T, \quad \eta = 1, 2, 3 \tag{55b}$$

$$\mathbf{F}_{fe} = [F^1, F^2, F^3] \tag{55c}$$

$$\mathbf{F}^\eta = [F_1^\eta, F_2^\eta, F_3^\eta, M_1^\eta, M_2^\eta, M_3^\eta, M_\phi^\eta]^T \tag{55d}$$

where $\mathbf{U}^\eta$ and $\mathbf{F}^\eta$ are the nodal point displacement and force vectors, respectively.

Substituting the shape functions and cross-sectional properties into Eqs. (6), (11), (12) and integrating along the element length, the total potential energy of the thin-walled finite curved beam element is obtained in a matrix form as

$$\Pi_T = \frac{1}{2}\mathbf{U}_{fe}^T(\mathbf{K}_{fe}^e + \mathbf{K}_{fe}^f + \mathbf{K}_{fe}^g)\mathbf{U}_{fe} - \mathbf{U}_{fe}^T\mathbf{F}_{fe} \tag{56}$$

where $\mathbf{K}_{fe}^e$ and $\mathbf{K}_{fe}^f$ are the element elastic stiffness matrix and the stiffness matrix considering the foundation effects, respectively, in local coordinate; $\mathbf{K}_{fe}^g$ is the geometric stiffness matrix. Stiffness matrices are evaluated using a reduced Gauss numerical integration scheme and the assembly of element stiffness matrix for the entire structure based on the coordinate transformation leads to the equilibrium matrix equation in a global coordinate system. Here it should be noted that the element displacement and force vectors of an isoparametric curved beam are identical to those of the present curved beam but interpolation functions are different.

5. Numerical examples

To demonstrate accuracy and validity of the proposed stiffness matrices of curved beam, the present stability analyses of curved beams resting on elastic foundation subjected to uniform compression and pure bending are performed and compared with the finite element solutions using the classical isoparametric curved beam elements and other researchers' analytical solutions. Also for the stability analysis of curved beam neglecting the shear deformation effect, the Hermitian curved beam element developed by Kim *et al.* (2000b) which defines all seven displacement parameters at centroid is used. In their study, the third order Hermitian polynomials are adopted to interpolate all displacement parameters. The analytical expressions by other researchers for in-plane buckling loads of curved beam subjected to uniform compression and for lateral buckling loads of beam subjected to pure bending, which restrict to the case neglecting the shear deformation and the second-order terms of semi-tangential rotations, are presented in the study by Kim *et al.* (2000a).

5.1 In-plane and lateral buckling of curved beam with doubly symmetric cross-section

Fig. 4 shows the doubly symmetric cross-section and its material and sectional properties of curved beam on elastic foundation subjected to uniform compression and pure bending. The beam is supported simply at two ends and the length is 1.0 m. First, for the curved beam without elastic foundation, the in-plane buckling loads of the curved beam subjected to uniform compression with various subtended angle is evaluated by keeping the length of curved beam constant. In Table 1, the in-plane antisymmetric buckling loads obtained from this study are presented and compared with other analytical solutions. It can be found from Table 1 that the in-plane bucking loads evaluated by present stiffness matrix method (SMM) using a single element coincide with the results from 30 isoparametric curved beam elements for whole ranges of subtended angles considered. Due to the shear effects, the buckling loads are shown to decrease about 25% and the present solutions without shear effects deviates somewhat from the previously published analytical results for larger angle due to the different formulation of stability equations. It is noted that the results obtained from this curved beam model with shear effects have been compared with results obtained from shell elements in the paper by Kim *et al.* (2005) and very good agreement between two solutions is
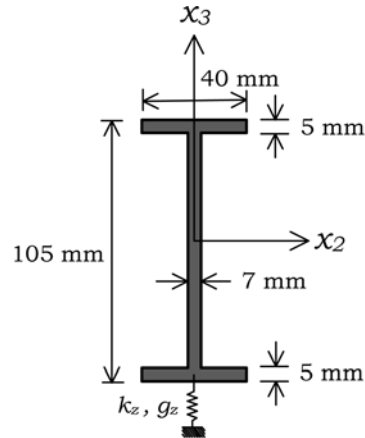
(a) Doubly symmetric cross-section

$E = 730$ N/mm², $G = 280$ N/mm², $A = 1100$ mm², $J = 14766.7$ mm⁴

$I_2 = 1583333.3$ mm⁴, $I_3 = 53333.3$ mm⁴, $I_\phi = 133333333$ mm⁶, $I_{\phi 23} = -133333333$ mm⁶

$A_2 = 333.333$ mm², $A_3 = 657.662$ mm², $A_r = 833333.3$ mm⁴

(b) Material and sectional properties

Fig. 4 Doubly symmetric cross-section and its material, sectional properties

Table 1 In-plane antisymmetric buckling loads F_{1cr} for the SS doubly symmetric I-beam subjected to uniform compression (N)

ψ (°)	This study			Rajasekaran and Padmanabhan (1989)
	SMM	30 Isoparametric beam elements	Without shear	
30	36554.0	36554.0	45607.0	45311.0
60	36466.0	36466.0	45488.0	44328.0
90	36165.0	36166.0	45100.0	42601.0
180	29801.0	29801.0	37171.0	31590.0
270	8371.8	8371.9	10443.0	11585.0
360	0.0	0.0	0.0	0.0

Table 2 In-plane buckling loads F_{1cr} for the SS doubly symmetric I-beam subjected to uniform compression (N), ($l = 1.0$ m, $\psi = 90°$)

Mode	Isoparametric beam elements						SMM
	4	6	8	10	20	30	
1	36600.0	36256.4	36194.9	36177.6	36166.2	36165.5	36165.4
2	68083.6	65853.1	65437.3	65317.6	65236.6	65232.1	65231.0
3	100415.0	93467.2	92132.7	91738.3	91464.8	91449.3	91445.4
4	129980.0	115826.0	113014.0	112163.0	111557.0	111521.0	111513.0
5	151837.0	134368.0	129605.0	128126.0	127045.0	126980.0	126964.0

Table 3 In-plane buckling loads F_{1cr} for the SC doubly symmetric I-beam subjected to uniform compression (N), (l = 1.0 m, ψ = 90°)

Mode	Isoparametric beam elements						SMM
	4	6	8	10	20	30	
1	47874.5	47134.3	46999.1	46960.8	46935.3	46933.9	46933.5
2	75088.9	72193.2	71645.3	71486.4	71378.3	71372.2	71370.8
3	107499.0	99720.5	98163.8	97697.6	97371.2	97352.5	97347.8
4	131384.0	117981.0	115180.0	114321.0	113704.0	113668.0	113659.0
5	156317.0	135832.0	131249.0	129798.0	128726.0	128661.0	128644.0

(a) 1st mode

(b) 2nd mode

(c) 3rd mode
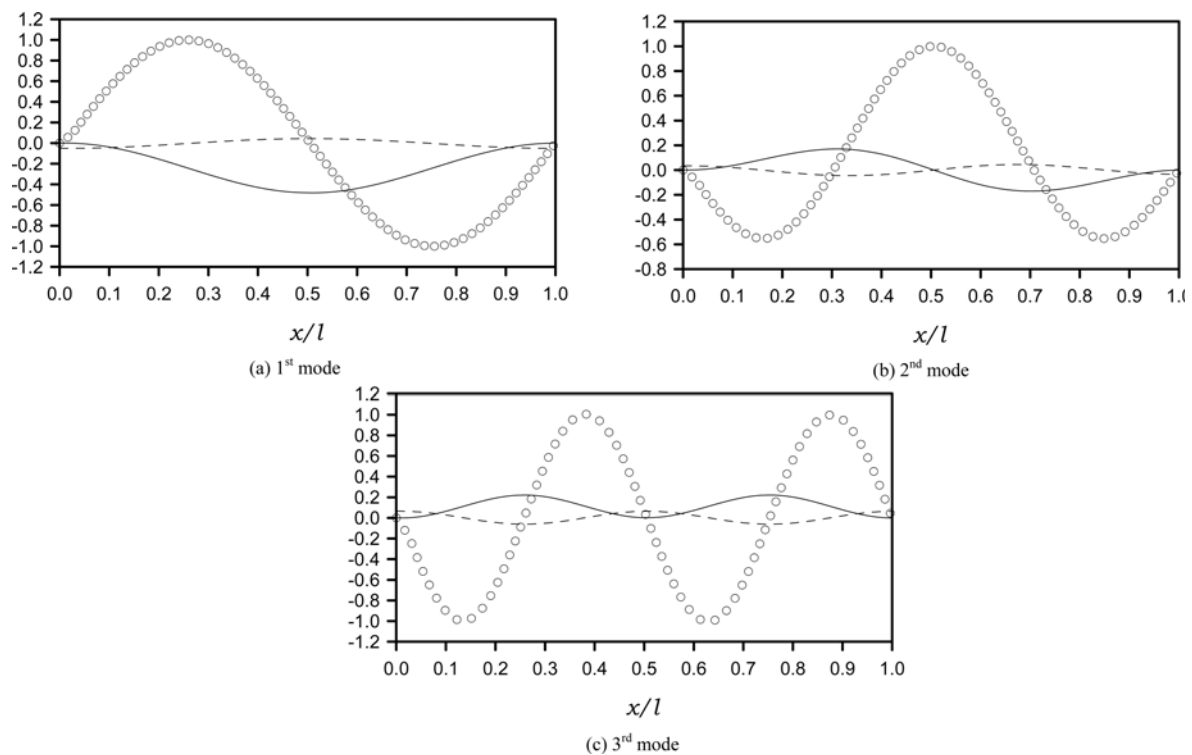
Fig. 5 Mode shapes corresponding to the in-plane buckling loads of SS beam: (solid line), U_z (circle symbol), and ω_2 (dashed line)

observed. For simply supported (SS) and simply-clamped (SC) curved beams with subtended angle ψ = 90°, the lowest five in-plane buckling loads by SMM and by finite element solutions using various numbers of isoparametric curved beam elements are presented in Tables 2 and 3, respectively. It is shown from Tables 2 and 3 that the results using as many as 30 isoparametric beam elements are in excellent agreement with the solutions from SMM. It should be noted that the present numerical method gives the accurate results for the higher buckling modes as well as the lower ones because the displacement state vector satisfies the homogeneous form of the equilibrium equations. It is observed that a large number of isoparametric beam elements need to be used to obtain sufficiently accurate results especially for the higher buckling modes. Fig. 5 shows the mode
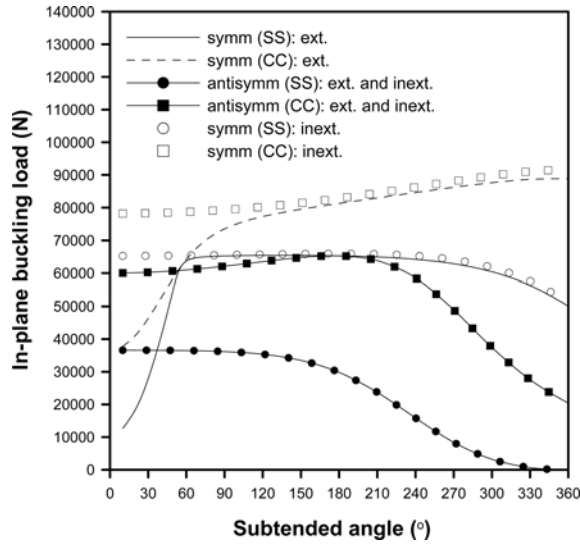
Fig. 6 In-plane bucking load of curved I-beam subjected to uniform compression under the assumption of extensional and inextensional conditions ($l = 1.0$ m)
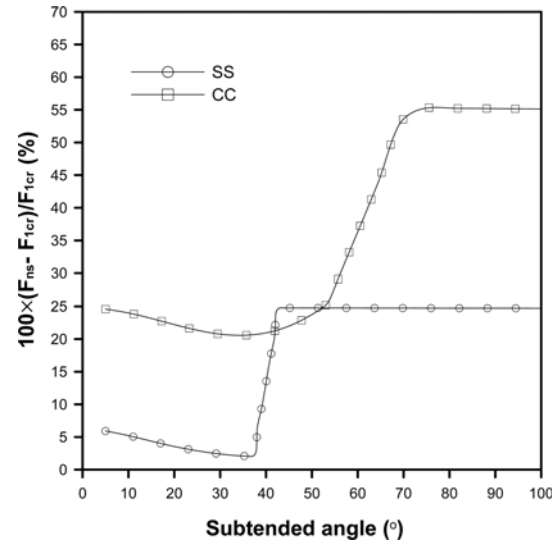
Fig. 7 Variation of shear deformation effect on the fundamental in-plane bucking load of curved I-beam

shapes corresponding to the first three in-plane buckling loads of SS beam. It can be observed from Fig. 5 that the relative magnitude of the axial displacement component (solid line) to the flexural one in the x_3-direction (dashed line) is the largest for the 1st mode but its value of the rotational angle (dashed line) to the flexural one is the largest for the 3rd mode.

To investigate the variation of buckling loads, the fundamental in-plane symmetric and antisymmetric buckling loads of the simply supported (SS) and clamped (CC) beams with respect to the subtended angles under the assumptions of extensional and inextensional conditions are depicted in Fig. 6. For the inextensional condition, the constraint of $U_x' + U_z/R \approx 0$ is imposed on the elastic strain and geometric potential energies in Eqs. (6) and (12). It can be observed from Fig. 6 that there exists a crossover of subtended angle at which the buckling mode changes from symmetric to antisymmetric. For SS beam under extensional condition, the lowest buckling mode is symmetric for $\psi < 37.5°$ but changes to antisymmetric mode for $\psi > 37.5°$. A similar crossover phenomenon is also seen for CC beam under the extensional condition at $\psi = 53.6°$. Fig. 7 shows the relative difference of the fundamental in-plane buckling loads due to shear effects with the increase of subtended angles. It is interesting to note that effect of shear deformation increases sharply around the crossover angle. In range with smaller subtended angle, the effect of shear is relatively small because the fundamental buckling mode corresponds to the symmetric mode with one half-wave. With the subtended angle larger than the crossover angle, however, the fundamental mode changes into the antisymmetric one with two half-waves, where the shear effect becomes greater. The detailed explanation of this buckling mode transformation phenomenon is described in the study by Kim *et al.* (2005). It can also be found from Fig. 6 that as the subtended angle increases, the symmetric buckling load under the extensional condition approaches that under the inextensional condition at subtended angles of around 64° and 171° for SS and CC beams, respectively. Two buckling loads become identical with the further increase of the subtended angle.
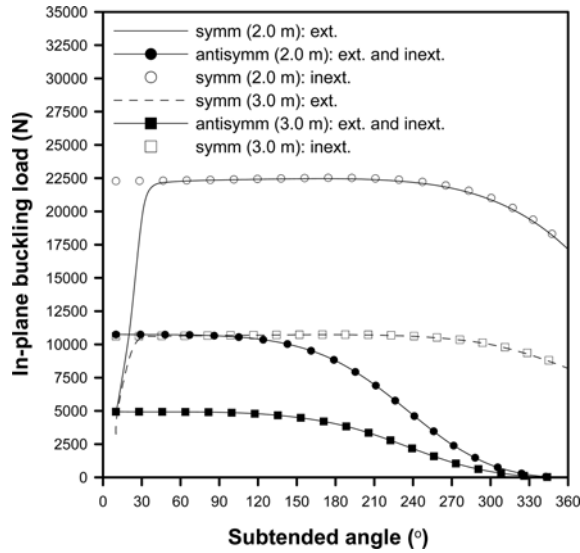
Fig. 8 In-plane bucking load of the SS curved I-beam subjected to uniform compression under the assumption of extensional and inextensional conditions (l = 2.0 m and 3.0 m)
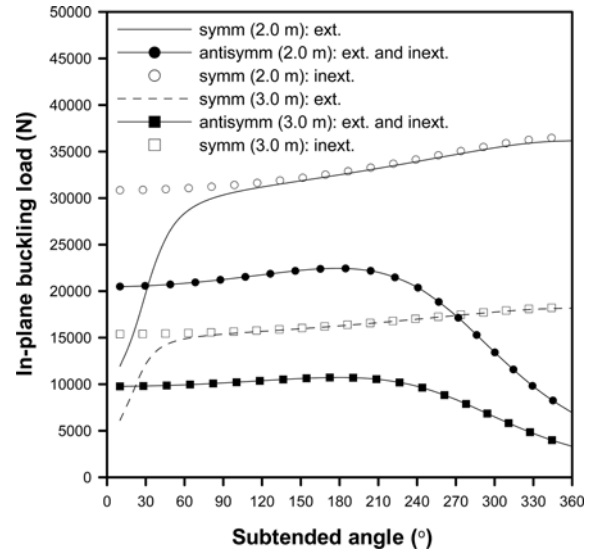
Fig. 9 In-plane bucking load of the CC curved I-beam subjected to uniform compression under the assumption of extensional and inextensional conditions (l = 2.0 m and 3.0 m)

Figs. 8 and 9 show the in-plane buckling load curves of SS and CC beams, respectively, for beams with the length of 2.0 m and 3.0 m. It is observed from Fig. 8 that the crossover from symmetric mode to antisymmetric one occurs at subtended angles of 18° and 12° for 2 m and 3 m long beams, respectively. Also the symmetric buckling load under the extensional condition and that under the inextensional condition become identical around 46° for 3.0 m long beam and 29° for 3.0 m long beam. For CC beam, as can be seen in Fig. 9, the crossover of buckling modes occurs at 30° and 22° and the buckling loads under the extensional and inextensional conditions put together after 135° for 2.0 m beam and 69° for 3.0 m beam. In Fig. 10, the variation of the crossover angle is shown with respect to the length of beam. Consequently, as the length of beam increases, the values of crossover angle from symmetric to antisymmetric buckling modes decrease and the values of merging points for buckling load under the extensional condition and that under the inextensional one decrease with an increase of beam length.

The influence of foundation parameters on the in-plane buckling behavior of curved beam is investigated. In-plane symmetric and antisymmetric buckling loads, which are not presented due to space limitation, increase as the Winkler type of foundation parameter k_z and the second type of foundation parameter g_z increase. Therefore k_z and g_z make the curved beam stiffer. In Figs. 11 and 12, the variation of crossover angle of in-plane buckling loads is shown with respect to k_z and g_z, respectively. From Fig. 11, it can be seen that the crossover angle decreases with increase of k_z for both boundary conditions. However, variation of crossover angle for curved beams considering g_z, as is shown in Fig. 12, is contrary to that considering k_z.

Next, for SS beam subjected to pure bending, the lateral buckling moments M_{2cr} by SMM are presented with the results from 30 isoparametric beam elements and the solutions neglecting shear effects in Table 4. Also given in Table 4 are analytical solutions by other researchers who did not consider the shear effects and the second-order terms of semi-tangential rotations. It can be found
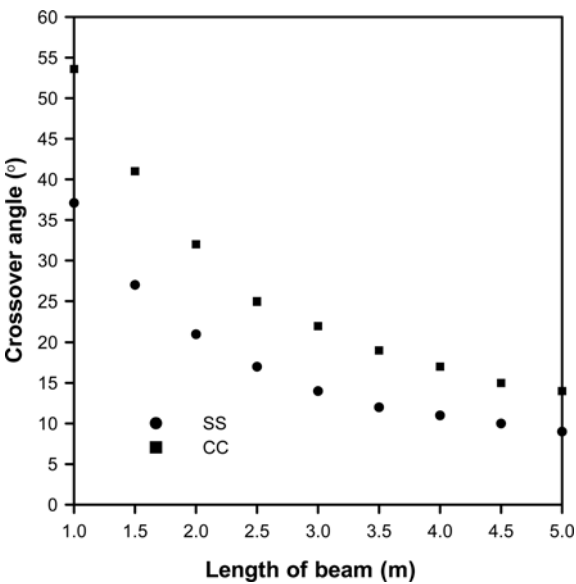
Fig. 10 Crossover angle of curved I-beam with respect to the length of beam
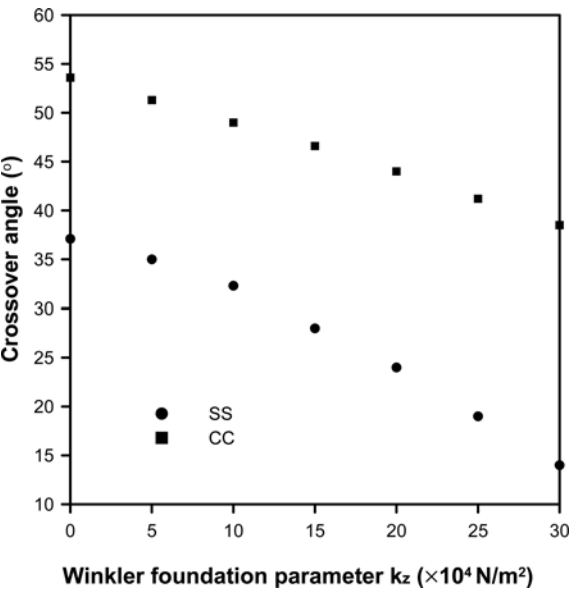
Fig. 11 Crossover angle of curved I-beam with respect to the Winker foundation parameter k_z
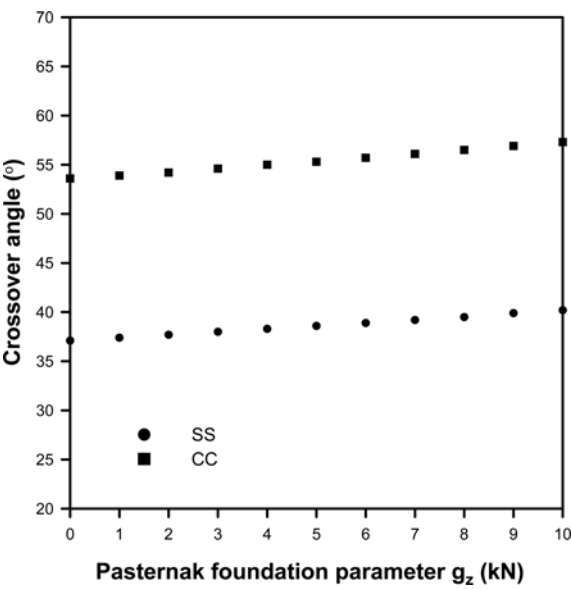
Fig. 12 Crossover angle of curved I-beam with respect to the second-type of foundation parameter g_z

from Table 4 that the results by SMM using only a single element are in excellent agreement with the finite element results using 30 beam elements. It is also found that because of the effects of shear deformations, the buckling moment for antisymmetric mode with subtended angle of 270° increases 17.10%.

Table 4 Lateral symmetric and antisymmetric buckling moments M_{2cr} for the SS double symmetric I-beam subjected to pure bending (Nm)

| Mode	ψ (°)	This study			Rajasekaran and Padmanabhan (1989)
		SMM	30 Isoparametric beam elements	Without shear	
Symm.	30	33.063	33.063	33.497	33.600
	60	23.936	23.936	24.484	24.610
	90	16.423	16.423	16.936	17.036
	180	0.0	0.0	0.0	0.0
	270	12.007	12.007	12.762	12.556
	360	22.412	22.414	24.159	23.174
Antisymm.	30	95.420	95.420	98.236	98.745
	60	82.595	82.596	86.500	87.348
	90	70.871	70.872	75.491	76.525
	180	41.437	41.438	46.344	47.250
	270	18.562	18.562	21.736	22.064
	360	0.0	0.0	0.0	0.0
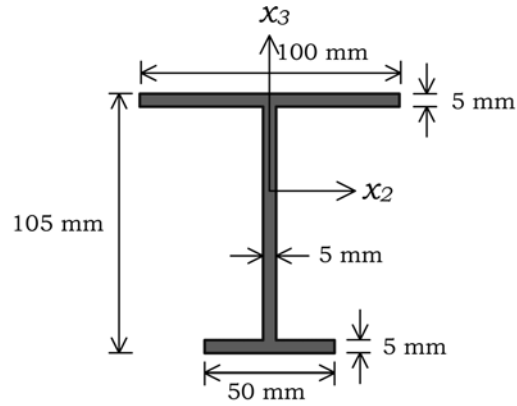
(a) Mono-symmetric cross-section

$E = 730$ N/mm^2, $G = 280$ N/mm^2, $A = 1250$ mm^2, $J = 10416.7$ mm^4

$I_2 = 2166667$ mm^4, $I_3 = 468750$ mm^4, $I_{222} = -35000000$ mm^5, $I_{233} = 13541667$ mm^5

$I_\phi = 854166667$ mm^6, $I_{\phi3} = -13541666$ mm^5, $I_{\phi23} = -854166666$ mm^6, $I_{\phi\phi2} = 15416666666$ mm^7

$A_2 = 511.364$ mm^2, $A_3 = 453.387$ mm^2, $A_r = 1815657.7$ mm^4, $A_{2r} = -14772.76$ mm^3

(b) Material and sectional properties

Fig. 13 Mono-symmetric cross-section and its material, sectional properties

5.2 Lateral buckling of curved beam with mono-symmetric cross-section

In this example, the SS curved beam with mono-symmetric cross-section, as shown in Fig. 13, is

Table 5 Lateral symmetric and antisymmetric buckling moments M_{2cr} for the SS mono-symmetric I-beam subjected to pure bending (Nm)

Mode	ψ (°)	This study			Trahair and Papangelis (1987)	Vlasov (1961)
		SMM	30 Isoparametric beam elements	Without shear		
Symm.	30	159.400	159.400	161.690	164.440	168.190
	60	79.355	79.355	80.066	76.481	84.863
	90	41.304	41.304	41.585	33.156	43.694
	180	0.0	0.0	0.0	0.0	0.0
Antisymm.	30	850.320	850.320	914.710	947.160	955.020
	60	689.580	689.590	736.110	787.300	804.410
	90	546.620	546.620	579.040	634.360	662.210
	180	242.420	242.420	252.530	251.680	313.570

considered. The beam is under pure bending and the length is 1.0 m. In Table 5, the lateral buckling moments obtained from this study with and without shear effects are presented for various subtended angles and compared with analytical solutions by Trahair and Papangelis (1987) and Vlasov (1961) in which the shear and thickness-curvature effects, the second terms of semi-tangential rotations, and the Wagner effect in evaluation of potential energy are neglected. These complicated effects on the buckling moments are more significant for the curved beam with larger subtended angle and smaller radius. It is observed from Table 5 that an excellent agreement between results from SMM using a single element and those from the finite element analysis using 30 isoparametric beam elements is evident. In this case, the maximum difference of buckling moments due to shear effect is 7.57% at angle of 30° for antisymmetric mode.

5.3 Spatially coupled buckling of curved beam with non-symmetric cross-section

The purpose of our final example is to evaluate the axially-flexurally-torsionally coupled buckling loads of curved beam with non-symmetric cross-section subjected to uniform compression and to investigate the influence of various foundation parameters on the coupled buckling behavior. The configuration of non- symmetric cross-section resting on elastic foundation and its material, sectional properties are shown in Fig. 14. The length of beam is 1.2 m and the boundary conditions are simply supported (SS) and simply-clamped (SC) at two ends. For SS and SC beams, the lowest three spatially coupled buckling loads by SMM neglecting foundation effects are presented and compared with the results from various numbers of isoparametric curved beam elements under extensional condition in Tables 6 and 7, respectively. It can be observed from Tables 6 and 7 that a large number of isoparametric beam elements are required to obtain sufficiently accurate buckling loads for the higher buckling modes and large subtended angles. In this case, the finite element solutions using at least 30 beam elements yield the reasonably good results in the higher buckling modes when compared with the results by SMM. In addition, the convergence study has been conducted for the coupled buckling loads of SS and SC beams with angle of 10° with respect to the increase of the number of terms in power series expansion and the buckling loads with various numbers of terms are presented in Tables 8 and 9, respectively. It is observed from Tables 8 and 9 that the coupled buckling loads gradually approach the solutions as the number n increases and the
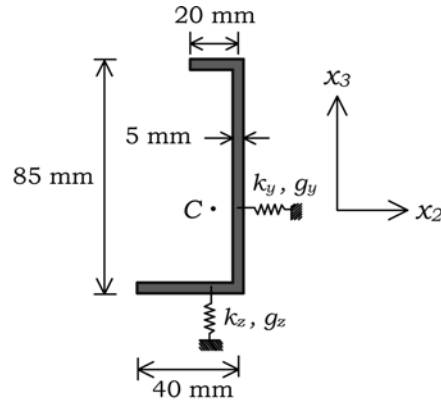
(a) Non-symmetric cross-section

$E = 730 \text{ N/mm}^2, \quad G = 280 \text{ N/mm}^2, \quad A = 700 \text{ mm}^2, \quad J = 5833.3 \text{ mm}^4, \quad l = 1200 \text{ mm}, \quad I_2 = 670476.2 \text{ mm}^4$

$I_3 = 84285.7 \text{ mm}^4, \quad I_{23} = 91428.6 \text{ mm}^4, \quad I_{222} = 5224490 \text{ mm}^5, \quad I_{223} = -2002721 \text{ mm}^5, \quad I_{233} = -1741497 \text{ mm}^5$

$I_{333} = -1338776 \text{ mm}^5, \quad I_\phi = 272544218 \text{ mm}^6, I_{\phi 2} = 11580952 \text{ mm}^5, \quad I_{\phi 3} = 3047619 \text{ mm}^5, \quad I_{\phi 22} = 59210884 \text{ cm}^6$

$I_{\phi 23} = -107102040 \text{ mm}^6, \quad I_{\phi\phi 2} = -671720116 \text{ mm}^7, \quad A_2 = 173.408 \text{ mm}^2, \quad A_3 = 344.097 \text{ mm}^2, \quad A_{23} = 26.622 \text{ mm}^2$

$A_r = 410932.4 \text{ mm}^4, \quad A_{2r} = 4182.60 \text{ mm}^3, \quad A_{3r} = 4463.84 \text{ mm}^3$

(b) Material and sectional properties

Fig. 14 Non-symmetric cross-section and its material, sectional properties

Table 6 Spatially coupled buckling loads F_{1cr} for the SS beam with non-symmetric cross-section subjected to uniform compression (N) (l = 1.2 m)

ψ (°)	Mode	Isoparametric beam elements					SMM	Without shear
		4	6	10	20	30		
10	1	254.54	254.34	254.29	254.29	254.29	254.29	255.62
	2	863.89	856.24	854.48	854.23	854.21	854.21	868.20
	3	1605.9	1547.1	1533.2	1531.0	1530.9	1530.9	1577.5
30	1	139.32	139.17	139.13	139.13	139.13	139.13	139.67
	2	663.61	656.25	654.56	654.31	654.30	654.30	663.19
	3	1409.0	1348.9	1334.7	1332.5	1332.4	1332.4	1371.0
60	1	57.328	57.237	57.217	57.215	57.215	57.214	57.437
	2	446.78	440.33	438.85	438.63	438.62	438.62	443.23
	3	1154.5	1095.2	1081.2	1079.1	1079.0	1079.0	1107.6
90	1	23.322	23.274	23.263	23.262	23.262	23.262	23.359
	2	301.30	295.98	294.77	294.59	294.58	294.58	297.00
	3	942.39	885.92	872.62	870.61	870.50	870.48	891.49
180	1	0.000014	0.0	0.0	0.0	0.0	0.0	0.0
	2	87.366	84.913	84.355	84.274	84.269	84.268	84.620
	3	495.48	452.99	443.12	441.64	441.55	441.53	449.23

Table 7 Spatially coupled buckling loads F_{1cr} for the SC beam with non-symmetric cross-section subjected to uniform compression (N) ($l = 1.2$ m)

ψ (°)	Mode	Isoparametric beam elements					SMM	Without shear
		4	6	10	20	30		
10	1	505.05	503.48	503.13	503.08	503.08	503.08	508.94
	2	1188.8	1166.9	1161.8	1161.0	1161.0	1161.0	1187.9
	3	2041.5	1917.4	1887.6	1883.0	1882.8	1882.7	1957.4
30	1	381.22	379.46	379.06	379.01	379.00	379.00	383.25
	2	1018.7	995.04	989.49	988.66	988.62	988.61	1010.3
	3	1882.2	1749.2	1717.7	1712.9	1712.6	1712.5	1779.9
60	1	271.73	269.60	269.12	269.05	269.05	269.05	272.27
	2	852.29	824.98	818.54	817.58	817.53	817.51	835.45
	3	1695.5	1552.9	1519.0	1513.8	1513.5	1513.4	1571.7
90	1	195.07	192.79	192.27	192.20	192.19	192.19	194.72
	2	734.24	702.70	695.25	694.13	694.07	694.06	710.71
	3	1562.1	1406.3	1369.1	1363.3	1363.0	1362.9	1416.5
180	1	64.104	62.569	62.221	62.171	62.168	62.167	63.090
	2	436.76	402.61	394.66	393.47	393.41	393.39	404.05
	3	1234.4	1036.8	990.75	983.62	983.21	983.11	1026.7

Table 8 Convergence of the coupled buckling loads for the SS non-symmetric beam with the increase of n ($\psi = 10°$)

Mode	Number of terms in power series expansion, n							
	8	10	15	20	25	27	28	30
1	244.41	255.22	254.28	254.29	254.29	254.29	254.29	254.29
2	-	-	-	854.42	854.21	854.21	854.21	854.21
3	-	-	-	-	-	1534.9	1530.5	1530.9

Table 9 Convergence of the coupled buckling loads for the SC non-symmetric beam with the increase of n ($\psi = 10°$)

Mode	Number of terms in power series expansion, n							
	8	10	15	20	25	28	30	35
1	-	429.0	501.9	503.08	503.08	503.08	503.08	503.08
2	-	-	-	-	1161.1	1161.0	1161.0	1161.0
3	-	-	-	-	-	-	1172.3	1182.7

convergence speed of SS beam is faster than that of SC beam.

Finally, the influence of foundation parameters on the coupled buckling behavior of non-symmetric beam is investigated. In evaluation of the foundation parameters, the analytical method studied by Vallabhan and Das (1991) based on the modified 2-D Vlasov model is applied. This method uses experimentally determined values for the soil modulus of elasticity E_s and the Poisson ratio v. If the soil is loose sand with $E_s = 0.175$ N/m^2 and $v = 0.28$, the application of the
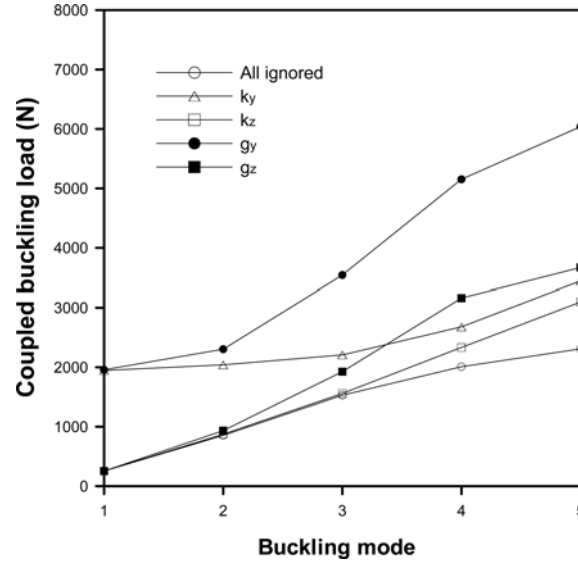
Fig. 15 Coupled buckling load of non-symmetric SS beam with various foundation parameters

Vallabhan-Das method produces the coefficient of sub-grade reaction $K_s = 994610$ N/m^3 and $g_y = g_z$ $= 14918520$ N. For a beam width $b_B = 40$ mm and height $h_B = 80$ mm, the Winkler foundation modulus are $k_y = K_s h_B = 79570$ N/m^2 and $k_z = K_s b_B = 39780$ N/m^2, respectively. For SS beam with the subtended angle of 10°, the spatially coupled buckling loads with various cases of foundation parameters are presented in Fig. 15. As shown in Fig. 15, the Winkler type of foundation parameters, k_y, k_z and the second type of ones, g_y, g_z increase the stiffness of curved beam and the effect of g_y is seen to be the most significant.

6. Conclusions

The series solutions for the axially, flexurally, and torsionally coupled buckling analysis of the thin-walled Timoshenko curved beam with non-symmetric cross-section on elastic foundation are presented based on the power series expansion of displacement components. As a special case, for beams with mono-symmetric and doubly symmetric cross-sections, these coupled series solutions are simplified to the solutions for in-plane buckling of curved beam subjected to uniform compression allowing the extension of centroid and the lateral buckling of beam subjected to pure bending. Through the numerical examples, it is demonstrated that results from this stiffness matrix method using only a single element have shown to be in excellent agreement with the solutions using a large number of isoparametric curved beam elements. Additionally, the coupling of symmetric and anti-symmetric modes at the in-plane buckling load crossover with change in curvature of beam is investigated. Through numerical examples considered, following conclusions may be drawn.
(1) As the length of curved beam increases, the value of crossover subtended angle from symmetric mode to antisymmetric buckling mode decreases. Also the value of merging point for buckling load under the extensional condition and that under the inextensional one

decreases with increase of beam length.

(2) The in-plane symmetric and antisymmetric buckling loads increase as the values of k_z and g_z increase.

(3) The value of crossover angle decreases with increase of k_z and increases with increase of g_z.

(4) The shear effect on lateral buckling moment, for beam with doubly symmetric cross-section, increases as the subtended angle increases. However, it decreases with the increase of subtended angle for mono-symmetric cross-section.

It is believed that proposed curved beam element based on the stiffness matrix is free from the shear locking since the displacement functions employed herein satisfy the homogenous form of the equilibrium equations. Furthermore, the current curved beam element eliminates discretization errors and is capable of predicting an infinite number of buckling loads of curved beams by means of a finite number of coordinates. Also this procedure is general enough to provide a systematic tool for exact solutions of simultaneous ordinary differential equations of the higher order with variable coefficients.

References

Aköz, A.Y. and Kadioğlu, F. (1996), "The mixed finite element solution of circular beam on elastic foundation", *Comput. Struct.*, **60**, 643-651.

Banan, M.R., Karami, G. and Farshad, M. (1989), "Finite element analysis of curved beams on elastic foundation", *Comput. Struct.*, **32**, 45-53.

Bathe, K.J. (1996), *Finite Element Procedures*. Englewood Cliffs, New York, Prentice-Hall.

Chakraborty, S. and Sarkar, S.K. (2000), "Analysis of a curved beam on uncertain elastic foundation" *Finite Elem. Anal. Des.*, **36**, 73-82.

Chang, S.P., Kim, M.Y. and Kim, S.B. (1996), "Stability of shear deformable thin-walled space frames and circular arches", *J. Eng. Mech.*, **122**, 844-854.

Choi, C.K. and Hong, H.S. (2001), "Finite strip analysis of multi-span box girder bridges by using non-periodic B-spline interpolation", *Struct. Eng. Mech.*, **12**, 313-328.

Chucheepsakul, S. and Saetiew, W. (2002), "Free vibrations of inclined arches using finite elements", *Struct. Eng. Mech.*, **13**, 713-730.

Dabrowski, R. (1968), *Curved Thin-walled Girders*. Cement and concrete association.

Dube, G.P. and Dumir, P.C. (1996), "Tapered thin open section beams on elastic foundation I. buckling analysis", *Comput. Struct.*, **61**, 845-857.

Heins, C.P. (1975), *Bending and Torsional Design in Structural Members*. D.C. Health and Company.

Hetenyi, M. (1946), *Beams on Elastic Foundations*. Scientific Series, Vol. XVI. Ann Arbor, University of Michigan Press.

Hu, N., Hu, B., Fukunaga, H. and Sekine, H. (1999), "Two kinds of C°-type elements for buckling analysis of thin-walled curved beams", *Comput. Meth. Appl. Mech. Eng.*, **171**, 87-108.

Kim, M.Y., Kim, N.I. and Kim, S.B. (2005), "Spatial stability of shear deformable curved beams with non-symmetric thin-walled sections. II: F.E. solutions and parametric study", *Comput. Struct.*, **83**, 2542-2558.

Kim, M.Y., Min, B.C. and Suh, M.W. (2000a), "Spatial stability of non-symmetric thin-walled curved beams I: analytical approach", *J. Eng. Mech.*, **126**, 497-505.

Kim, M.Y., Min, B.C. and Suh, M.W. (2000b), "Spatial stability of non-symmetric thin-walled curved beams II: Numerical approach", *J. Eng. Mech.*, **126**, 506-514.

Kim, M.Y., Kim, S.B. and Kim, N.I. (2005), "Spatial stability of shear deformable curved beams with non-symmetric thin-walled sections. I: Improved stability formulation", *Comput. Struct.*, **83**, 2525-2541.

Kim, N.I., Seo, K.J. and Kim, M.Y. (2003), "Free vibration and spatial stability of non-symmetric thin-walled curved beams with variable curvatures", *Int. J. Solids Struct.*, **40**, 3107-3128.

Lee, B.K., Oh, S.J. and Park, K.K. (2002), "Free vibrations of shear deformable circular curved beams resting on elastic foundations", *Int. J. Struct. Stab. Dyn.*, **2**, 77-97.

Papangelis, T.P. and Trahair, N.S. (1987), "Flexural-torsional buckling of arches", *J. Eng. Mech.*, **113**, 889-906.

Rajasekaran, S. and Padmanabhan, S. (1989), "Equations of curved beams", *J. Eng. Mech.*, **115**, 1094-1111.

Rodriquez, D.A. (1961), "Three-dimensional bending of a ring on an elastic foundation", *J. Appl. Mech.*, **28**, 461-463.

Saleeb, A.F. and Gendy, A.S. (1991), "Shear-flexible models for spatial bucking of thin-walled curved beams", *Int. J. Numer. Meth. Eng.*, **31**, 729-757.

Sengupta, D. and Dasgupta, S. (1987), "Horizontally curved isoparametric beam element with or without elastic foundation including effect of shear deformation", *Comput. Struct.*, **29**, 967-973.

Timoshenko, S.P. and Gere, J.M. (1961), *Theory of Elastic Stability, 2nd Ed.* New York: McGraw-Hill.

Trahair, N.S. and Papangelis, T.P. (1987), "Flexural-torsional buckling of monosymmetric arches", *J. Eng. Mech.*, **113**, 2271-2288.

Usuki, S., Kano, T. and Watanabe, N. (1979), "Analysis of thin walled curved members in account for large torsion", *Proc. JSCE*, **290**, 1-15.

Vallabhan, C.V.G. and Das, Y.C. (1991), "Modified Vlasov model for beans on elastic foundations", *J. Geotech. Eng.*, **117**, 956-966.

Vlasov, V.Z. (1961), *Thin-walled Elastic Beams, 2nd Ed.* National Science Foundation, Washington, D.C.

Wang, T.M. and Brannen, W.F. (1982), "Natural frequencies for out-of-plane vibrations of curved beams on elastic foundations", *J. Sound Vib.*, **84**, 241-246.

Watanabe, N., Kano, T. and Usuki, S. (1982), "Analysis of large torsion of a thin walled curved beam based on displacement field theory", *Proc. JSCE*, **317**, 31-45.

Wendroff, B. (1966), *Theoretical Numerical Analysis.* New York: Academic Press.

Wilson, J.F. and Lee, B.K. (1995), "In-plane free vibrations of catenary arches with unsymmetric axes", *Struct. Eng. Mech.*, **3**, 511-525.

Wilson, J.F., Lee, B.K. and Oh, S.J. (1994), "Free vibrations of circular arches with variable cross-section", *Struct. Eng. Mech.*, **2**, 345-357.

Wolfram, S. (2005), *Mathematica 5.2, a System for doing Mathematics by Computer.* Redwood City, California, Addison-Wesley.

Nam-Il Kim

Appendix A. Detailed components of $\mathbf{A_n}$, $\mathbf{B_n}$, and $\mathbf{S}$

1) Components of matrix $\mathbf{A_n}$

$$\mathbf{A_n} = \begin{bmatrix} \alpha_1 & \cdot & \cdot & \cdot & \alpha_2 & \alpha_3 & \alpha_4 \\ \cdot & \alpha_5 & \alpha_6 & \alpha_7 & \cdot & \cdot & \cdot \\ \cdot & -\alpha_6 & \alpha_8 & \alpha_9 & \cdot & \cdot & \cdot \\ \cdot & -\alpha_7 & \alpha_9 & \alpha_{10} & \cdot & \cdot & \cdot \\ \alpha_2 & \cdot & \cdot & \cdot & \alpha_{11} & \alpha_{12} & \alpha_{13} \\ \alpha_3 & \cdot & \cdot & \cdot & \alpha_{12} & \alpha_{14} & \alpha_{15} \\ \alpha_4 & \cdot & \cdot & \cdot & \alpha_{13} & \alpha_{15} & \alpha_{16} \end{bmatrix} \tag{A-1}$$

where

$$\alpha_1 = -\left(EA + \frac{E\hat{I}_2}{R^2} + {}^oF_1 - \frac{{}^oM_2}{R} \right)(n+2)(n+1), \quad \alpha_2 = \left(\frac{E\hat{I}_2}{R} - {}^oM_2 \right)(n+2)(n+1), \quad \alpha_3 = -\frac{E\hat{I}_{23}}{R}(n+2)(n+1)$$

$$\alpha_4 = \frac{E\hat{I}_{\phi 2}}{R}(n+2)(n+1), \quad \alpha_5 = \left(GA_2 + g_y + {}^oF_1 - \frac{{}^oM_2}{R} \right)(n+2)(n+1), \quad \alpha_6 = GA_{23}(n+2)(n+1)$$

$$\alpha_7 = \left(GA_{2r} - g_y h_z - {}^oM_2 \right)(n+2)(n+1), \quad \alpha_8 = -\left(GA_3 + g_z + {}^oF_1 - \frac{{}^oM_2}{R} \right)(n+2)(n+1)$$

$$\alpha_9 = -\left(GA_{3r} + g_z h_y \right)(n+2)(n+1), \quad \alpha_{10} = -\left(GJ + GA_r + g_y h_z^2 + g_z h_y^2 + \beta_1 {}^oF_1 + \beta_2 {}^oM_2 \right)(n+2)(n+1)$$

$$\alpha_{11} = -E\hat{I}_2(n+2)(n+1), \quad \alpha_{12} = E\hat{I}_{23}(n+2)(n+1), \quad \alpha_{13} = -E\hat{I}_{\phi 2}(n+2)(n+1), \quad \alpha_{14} = -E\hat{I}_3(n+2)(n+1)$$

$$\alpha_{15} = E\hat{I}_{\phi 3}(n+2)(n+1), \quad \alpha_{16} = -E\hat{I}_{\phi}(n+2)(n+1) \tag{A-2}$$

2) Components of matrix $\mathbf{B_n}$

$$\mathbf{B_n} = \begin{bmatrix} \gamma_1 & \cdot & \cdot & \gamma_2 & \cdot & \gamma_3 & \cdot & \gamma_4 & \gamma_5 & \cdot & \gamma_6 & \cdot & \gamma_7 & \cdot \\ \cdot & \gamma_2 & \gamma_8 & \cdot & \cdot & \cdot & \gamma_9 & \cdot & \cdot & \gamma_{10} & \cdot & \gamma_{11} & \cdot & \gamma_{12} \\ \cdot & -\gamma_3 & \cdot & \cdot & \gamma_{13} & \cdot & \gamma_{14} & \cdot & \cdot & \gamma_{15} & \cdot & \gamma_{16} & \cdot & \gamma_{17} \\ \cdot & -\gamma_4 & -\gamma_9 & \cdot & \gamma_{14} & \cdot & \gamma_{18} & \cdot & \cdot & \gamma_{19} & \cdot & \gamma_{20} & \cdot & \gamma_{21} \\ \gamma_5 & \cdot & \cdot & \gamma_{10} & \cdot & -\gamma_{15} & \cdot & -\gamma_{19} & \gamma_{22} & \cdot & \gamma_{23} & \cdot & \gamma_{24} & \cdot \\ \gamma_6 & \cdot & \cdot & \gamma_{11} & \cdot & \gamma_{16} & \cdot & -\gamma_{20} & \gamma_{23} & \cdot & \gamma_{25} & \cdot & \gamma_{26} & \cdot \\ \gamma_7 & \cdot & \cdot & \gamma_{12} & \cdot & -\gamma_{17} & \cdot & -\gamma_{21} & \gamma_{24} & \cdot & \gamma_{26} & \cdot & \gamma_{27} & \cdot \end{bmatrix} \tag{A-3}$$

where

$$\gamma_1 = -\frac{GA_3}{R^2} - \frac{{}^oF_1}{R^2} + \frac{{}^oM_2}{R^3}, \quad \gamma_2 = \frac{GA_{23}}{R}(n+1), \quad \gamma_3 = \left(\frac{EA}{R} + \frac{E\hat{I}_2}{R^3} + \frac{GA_3}{R} + \frac{2{}^oF_1}{R} - \frac{2{}^oM_2}{R^2} \right)(n+1)$$

$$\gamma_4 = -\left(\frac{E\hat{I}_{23}}{R^2} - \frac{GA_{3r}}{R} \right)(n+1), \quad \gamma_5 = \frac{GA_3}{R} - \frac{{}^oM_2}{R^2}, \quad \gamma_6 = -\frac{GA_{23}}{R} + \frac{GA_{3r}}{R^2}, \quad \gamma_7 = \frac{GA_{3r}}{R}, \quad \gamma_8 = k_y, \quad \gamma_9 = -k_y h_z$$

$$\gamma_{10} = -GA_{23}(n+1), \quad \gamma_{11} = \left(GA_2 - \frac{GA_{2r}}{R}\right)(n+1), \quad \gamma_{12} = -GA_{2r}(n+1), \quad \gamma_{13} = -\frac{EA}{R^2} - \frac{EI_2}{R^4} - k_z - \frac{{}^oF_1}{R^2} + \frac{{}^oM_2}{R^3}$$

$$\gamma_{14} = \frac{E\hat{I}_{23}}{R^3} - k_z h_y, \quad \gamma_{15} = \left(\frac{E\hat{I}_2}{R^2} + GA_3 - \frac{2{}^oM_2}{R}\right)(n+1), \quad \gamma_{16} = -\left(\frac{E\hat{I}_{23}}{R^2} + GA_{23} - \frac{GA_{3r}}{R}\right)(n+1)$$

$$\gamma_{17} = \left(\frac{E\hat{I}_{\phi2}}{R^2} + GA_{3r}\right)(n+1), \quad \gamma_{18} = -\frac{E\hat{I}_3}{R^2} - k_y h_z^2 - k_z h_y^2 - k_\omega + \frac{{}^oM_2}{R}, \quad \gamma_{19} = -\left(\frac{E\hat{I}_{23}}{R} - GA_{3r}\right)(n+1)$$

$$\gamma_{20} = \left(\frac{E\hat{I}_3}{R} + \frac{GJ}{R} + \frac{GA_r}{R} - GA2_r + \frac{\beta_1{}^oF_1}{R} + \frac{\beta_2{}^oM_2}{R}\right)(n+1), \quad \gamma_{21} = -\left(\frac{E\hat{I}_{\phi3}}{R} - GA_r\right)(n+1), \quad \gamma_{22} = -GA_3$$

$$\gamma_{23} = GA_{23} - \frac{GA_{3r}}{R}, \quad \gamma_{24} = -GA_{3r}, \quad \gamma_{25} = -\frac{GJ}{R^2} - GA_2 - \frac{GA_r}{R^2} + 2\frac{GA_{2r}}{R} - \frac{\beta_1{}^oF_1}{R^2} - \frac{\beta_2{}^oM_2}{R^2}$$

$$\gamma_{26} = GA_{2r} - \frac{GA_r}{R}, \quad \gamma_{27} = -GA_r \tag{A-4}$$

3) Components of matrix **S**

$$\mathbf{S} = \begin{bmatrix} \cdot & s_1 & \cdot & \cdot & s_2 & \cdot & s_3 & \cdot & \cdot & s_4 & \cdot & s_5 & \cdot & s_6 \\ s_7 & \cdot & \cdot & s_8 & \cdot & s_9 & \cdot & s_{10} & s_9 & \cdot & s_{11} & \cdot & s_{12} & \cdot \\ s_{13} & \cdot & \cdot & s_9 & \cdot & s_{14} & \cdot & s_{15} & s_{16} & \cdot & s_{17} & \cdot & s_{18} & \cdot \\ s_{19} & \cdot & \cdot & s_{10} & \cdot & s_{15} & \cdot & s_{20} & s_{18} & \cdot & s_{21} & \cdot & s_{22} & \cdot \\ \cdot & s_{23} & \cdot & \cdot & s_{24} & \cdot & s_{25} & \cdot & \cdot & s_{26} & \cdot & s_{27} & \cdot & s_{28} \\ \cdot & s_{25} & \cdot & \cdot & -s_3 & \cdot & s_{26} & \cdot & \cdot & s_{27} & \cdot & s_{29} & \cdot & s_{30} \\ \cdot & s_6 & \cdot & \cdot & s_{31} & \cdot & s_{32} & \cdot & \cdot & s_{28} & \cdot & s_{30} & \cdot & s_{33} \end{bmatrix} \tag{A-5}$$

where

$$s_1 = EA + \frac{E\hat{I}_2}{R^2} + {}^oF_1 - \frac{{}^oM_2}{R}, \quad s_2 = \frac{EA}{R} + \frac{E\hat{I}_2}{R^3} + \frac{{}^oF_1}{R} - \frac{{}^oM_2}{R^2}, \quad s_3 = -\frac{E\hat{I}_{23}}{R^2}, \quad s_4 = -\frac{E\hat{I}_2}{R}, \quad s_5 = \frac{E\hat{I}_{23}}{R} + {}^oM_2$$

$$s_6 = -\frac{E\hat{I}_{\phi2}}{R}, \quad s_7 = -\frac{GA_{23}}{R}, \quad s_8 = GA_2 + g_y + {}^oF_1 - \frac{{}^oM_2}{R}, \quad s_9 = GA_{23}, \quad s_{10} = GA_{2r} - g_y h_z - {}^oM_2$$

$$s_{11} = -GA_2 + \frac{GA_{2r}}{R}, \quad s_{12} = GA_{2r}, \quad s_{13} = -\frac{GA_3}{R} - \frac{{}^oF_1}{R} + \frac{{}^oM_2}{R^2}, \quad s_{14} = GA_3 + g_z + {}^oF_1 - \frac{{}^oM_2}{R}$$

$$s_{15} = GA_{3r} + g_z h_y, \quad s_{16} = GA_3, \quad s_{17} = -GA_{23} + \frac{GA_{3r}}{R} - \frac{{}^oM_2}{R}, \quad s_{18} = GA_{3r}, s_{19} = -\frac{GA_{3r}}{R}$$

$$s_{20} = GJ + GA_r + g_y h_z^2 + g_z h_y^2 + \beta_1{}^oF_1 + \beta_2{}^oM_2, \quad s_{21} = \frac{GJ}{R} + \frac{GA_r}{R} - GA_{2r} + \frac{\beta_1{}^oF_1}{R} + \frac{\beta_2{}^oM_2}{R} + 0.5{}^oM_2$$

$$s_{22} = GA_r, \quad s_{23} = -\frac{E\hat{I}_2}{R} + {}^oM_2, \quad s_{24} = -\frac{E\hat{I}_2}{R^2} + \frac{{}^oM_2}{R}, \quad s_{25} = \frac{E\hat{I}_{23}}{R}, \quad s_{26} = -\frac{E\hat{I}_3}{R} + 0.5{}^oM_2, \quad s_{27} = -E\hat{I}_{23}$$

$$s_{28} = E\hat{I}_{\phi2}, \quad s_{29} = E\hat{I}_3, \quad s_{30} = -E\hat{I}_{\phi3}, \quad s_{31} = -\frac{E\hat{I}_{\phi2}}{R^2}, \quad s_{32} = \frac{E\hat{I}_{\phi3}}{R}, \quad s_{33} = E\hat{I}_\phi \tag{A-6}$$

Appendix B. Expressions of N_1 and N_i

1) Components of matrix $\mathbf{N}_1$

$$\mathbf{N}_1 = \begin{bmatrix} \cdot & 1 & \cdot & \cdots\cdots & \cdot & \cdot & \cdot \\ L_2(1,1) & L_2(1,2) & L_2(1,3) & \cdots\cdots & L_2(1,12) & L_2(1,13) & L_2(1,14) \\ \cdot & \cdot & \cdot & \cdots\cdots & \cdot & \cdot & \cdot \\ L_2(2,1) & L_2(2,2) & L_2(2,3) & \cdots\cdots & L_2(2,12) & L_2(2,13) & L_2(2,14) \\ \cdot & \cdot & \cdot & \cdots\cdots & \cdot & \cdot & \cdot \\ L_2(3,1) & L_2(3,2) & L_2(3,3) & \cdots\cdots & L_2(3,12) & L_2(3,13) & L_2(3,14) \\ \cdot & \cdot & \cdot & \cdots\cdots & \cdot & \cdot & \cdot \\ L_2(4,1) & L_2(4,2) & L_2(4,3) & \cdots\cdots & L_2(4,12) & L_2(4,13) & L_2(4,14) \\ \cdot & \cdot & \cdot & \cdots\cdots & \cdot & \cdot & \cdot \\ L_2(5,1) & L_2(5,2) & L_2(5,3) & \cdots\cdots & L_2(5,12) & L_2(5,13) & L_2(5,14) \\ \cdot & \cdot & \cdot & \cdots\cdots & 1 & \cdot & \cdot \\ L_2(6,1) & L_2(6,2) & L_2(6,3) & \cdots\cdots & L_2(6,12) & L_2(6,13) & L_2(6,14) \\ \cdot & \cdot & \cdot & \cdots\cdots & \cdot & \cdot & 1 \\ L_2(7,1) & L_2(7,2) & L_2(7,3) & \cdots\cdots & L_2(7,12) & L_2(7,13) & L_2(7,14) \end{bmatrix} \tag{A-7}$$

2) Components of matrix $\mathbf{N}_i$

$$\mathbf{N}_i = \begin{bmatrix} L_i(1,1) & L_i(1,2) & L_i(1,3) & \cdots\cdots & L_i(1,12) & L_i(1,13) & L_i(1,14) \\ L_{i+1}(1,1) & L_{i+1}(1,2) & L_{i+1}(1,3) & \cdots\cdots & L_{i+1}(1,12) & L_{i+1}(1,13) & L_{i+1}(1,14) \\ L_i(2,1) & L_i(2,2) & L_i(2,3) & \cdots\cdots & L_i(2,12) & L_i(2,13) & L_i(2,14) \\ L_{i+1}(2,1) & L_{i+1}(2,2) & L_{i+1}(2,3) & \cdots\cdots & L_{i+1}(2,12) & L_{i+1}(2,13) & L_{i+1}(2,14) \\ L_i(3,1) & L_i(3,2) & L_i(3,3) & \cdots\cdots & L_i(3,12) & L_i(3,13) & L_i(3,14) \\ L_{i+1}(3,1) & L_{i+1}(3,2) & L_{i+1}(3,3) & \cdots\cdots & L_{i+1}(3,12) & L_{i+1}(3,13) & L_{i+1}(3,14) \\ L_i(4,1) & L_i(4,2) & L_i(4,3) & \cdots\cdots & L_i(4,12) & L_i(4,13) & L_i(4,14) \\ L_{i+1}(4,1) & L_{i+1}(4,2) & L_{i+1}(4,3) & \cdots\cdots & L_{i+1}(4,12) & L_{i+1}(4,13) & L_{i+1}(4,14) \\ L_i(5,1) & L_i(5,2) & L_i(5,3) & \cdots\cdots & L_i(5,12) & L_i(5,13) & L_i(5,14) \\ L_{i+1}(5,1) & L_{i+1}(5,2) & L_{i+1}(5,3) & \cdots\cdots & L_{i+1}(5,12) & L_{i+1}(5,13) & L_{i+1}(5,14) \\ L_i(6,1) & L_i(6,2) & L_i(6,3) & \cdots\cdots & L_i(6,12) & L_i(6,13) & L_i(6,14) \\ L_{i+1}(6,1) & L_{i+1}(6,2) & L_{i+1}(6,3) & \cdots\cdots & L_{i+1}(6,12) & L_{i+1}(6,13) & L_{i+1}(6,14) \\ L_i(7,1) & L_i(7,2) & L_i(7,3) & \cdots\cdots & L_i(7,12) & L_i(7,13) & L_i(7,14) \\ L_{i+1}(7,1) & L_{i+1}(7,2) & L_{i+1}(7,3) & \cdots\cdots & L_{i+1}(7,12) & L_{i+1}(7,13) & L_{i+1}(7,14) \end{bmatrix} \tag{A-8}$$

where $L_i(j,k)$ denote the component of L_i at j^{th} row and k^{th} column

Appendix C. Detailed components of $\mathbf{A_n^{in}}$ and $\mathbf{B_n^{in}}$

1) Components of matrix $\mathbf{A_n^{in}}$

$$\mathbf{A_n^{in}} = \begin{bmatrix} \hat{\alpha}_1 & \cdot & \hat{\alpha}_2 \\ \cdot & \hat{\alpha}_3 & \cdot \\ \hat{\alpha}_2 & \cdot & \hat{\alpha}_4 \end{bmatrix} \tag{A-9}$$

where

$$\hat{\alpha}_1 = -\left(EA + \frac{E\hat{I}_2}{R^2} + {}^oF_1\right)(n+2)(n+1), \quad \hat{\alpha}_2 = \frac{E\hat{I}_2}{R}(n+2)(n+1)$$

$$\hat{\alpha}_3 = -(GA_3 + g_z + {}^oF_1)(n+2)(n+1), \quad \hat{\alpha}_4 = -E\hat{I}_2(n+2)(n+1) \tag{A-10}$$

2) Components of matrix $\mathbf{B_n^{in}}$

$$\mathbf{B_n^{in}} = \begin{bmatrix} \hat{\gamma}_1 & \cdot & \cdot & \hat{\gamma}_2 & \hat{\gamma}_3 & \cdot \\ -\hat{\gamma}_2 & \cdot & \hat{\gamma}_4 & \cdot & \cdot & \hat{\gamma}_5 \\ \hat{\gamma}_3 & \cdot & \cdot & -\hat{\gamma}_5 & \hat{\gamma}_6 & \cdot \end{bmatrix} \tag{A-11}$$

where

$$\hat{\gamma}_1 = -\frac{GA_3}{R^2} - \frac{{}^oF_1}{R^2}, \quad \hat{\gamma}_2 = \left(\frac{EA}{R} + \frac{E\hat{I}_2}{R^3} + \frac{GA_3}{R} + \frac{2{}^oF_1}{R}\right)(n+1), \quad \hat{\gamma}_3 = \frac{GA_3}{R}$$

$$\hat{\gamma}_4 = -\frac{EA}{R^2} - \frac{E\hat{I}_2}{R^4} - k_z - \frac{{}^oF_1}{R^2}, \quad \hat{\gamma}_5 = \left(\frac{E\hat{I}_2}{R^2} + GA_3\right)(n+1), \quad \hat{\gamma}_6 = -GA_3 \tag{A-12}$$

Appendix D. Detailed components of $\mathbf{A}_n^{out}$ and $\mathbf{B}_n^{out}$

1) Components of matrix $\mathbf{A}_n^{out}$

$$\mathbf{A}_n^{out} = \begin{bmatrix} \tilde{\alpha}_1 & \tilde{\alpha}_2 & \cdot & \cdot \\ -\tilde{\alpha}_2 & \tilde{\alpha}_3 & \cdot & \cdot \\ \cdot & \cdot & \tilde{\alpha}_4 & \tilde{\alpha}_5 \\ \cdot & \cdot & \tilde{\alpha}_5 & \tilde{\alpha}_6 \end{bmatrix} \qquad (\text{A-13})$$

where

$$\tilde{\alpha}_1 = \left(GA_2 + g_y + {}^oF_1 - \frac{{}^oM_2}{R} \right)(n+2)(n+1), \qquad \tilde{\alpha}_2 = \left(GA_{2r} - g_y h_z - {}^oM_2 \right)(n+2)(n+1)$$

$$\tilde{\alpha}_3 = -\left(GJ + GA_r + g_y h_z^2 + g_z h_y^2 + \beta_1 {}^oF_1 + \beta_2 {}^oM_2 \right)(n+2)(n+1), \quad \tilde{\alpha}_4 = -E\hat{I}_3(n+2)(n+1)$$

$$\tilde{\alpha}_5 = E\hat{I}_{\phi3}(n+2)(n+1), \qquad \tilde{\alpha}_6 = -E\hat{I}_\phi(n+2)(n+1) \qquad (\text{A-14})$$

2) Components of matrix $\mathbf{B}_n^{out}$

$$\mathbf{B}_n^{out} = \begin{bmatrix} \tilde{\gamma}_1 & \cdot & \tilde{\gamma}_2 & \cdot & \cdot & \tilde{\gamma}_3 & \cdot & \tilde{\gamma}_4 \\ -\tilde{\gamma}_2 & \cdot & \tilde{\gamma}_5 & \cdot & \cdot & \tilde{\gamma}_6 & \cdot & \tilde{\gamma}_7 \\ \cdot & \tilde{\gamma}_3 & \cdot & -\tilde{\gamma}_6 & \tilde{\gamma}_8 & \cdot & \tilde{\gamma}_9 & \cdot \\ \cdot & \tilde{\gamma}_4 & \cdot & -\tilde{\gamma}_7 & \tilde{\gamma}_9 & \cdot & \tilde{\gamma}_{10} & \cdot \end{bmatrix} \qquad (\text{A-15})$$

where

$$\tilde{\gamma}_1 = k_y, \quad \tilde{\gamma}_2 = -k_y h_z, \quad \tilde{\gamma}_3 = \left(GA_2 - \frac{GA_{2r}}{R} \right)(n+1), \quad \tilde{\gamma}_4 = -GA_{2r}(n+1)$$

$$\tilde{\gamma}_5 = -\frac{E\hat{I}_3}{R^2} - k_y h_z^2 - k_z h_y^2 - k_\omega + \frac{{}^oM_2}{R}, \quad \tilde{\gamma}_6 = \left(\frac{E\hat{I}_3}{R} + \frac{GJ}{R} + \frac{GA_r}{R} - GA2_r + \frac{\beta_1 {}^oF_1}{R} + \frac{\beta_2 {}^oM_2}{R} \right)(n+1)$$

$$\tilde{\gamma}_7 = -\left(\frac{E\hat{I}_{\phi3}}{R} - GA_r \right)(n+1), \quad \tilde{\gamma}_8 = -\frac{GJ}{R^2} - GA_2 - \frac{GA_r}{R^2} + 2\frac{GA_{2r}}{R} - \frac{\beta_1 {}^oF_1}{R^2} - \frac{\beta_2 {}^oM_2}{R^2}$$

$$\tilde{\gamma}_9 = GA_{2r} - \frac{GA_r}{R}, \quad \tilde{\gamma}_{10} = -GA_r \qquad (\text{A-16})$$